
ASTEROID MINING: ACT&FRIENDS' RESULTS FOR THE GTOC 12 PROBLEM

A PREPRINT

Dario Izzo

European Space Technology and Research Centre
Noordwijk 2201 AZ, Netherlands
dario.izzo@esa.int

Marcus Märtens

European Space Technology and Research Centre
Noordwijk 2201 AZ, Netherlands

Laurent Beauregard

European Space Operations Centre
Darmstadt, 64293, Germany

Max Bannach

European Space Technology and Research Centre
Noordwijk 2201 AZ, Netherlands

Giacomo Acciarini

Surrey Space Center, University of Surrey
GU27XH, Guildford, United Kingdom

Emmanuel Blazquez

European Space Technology and Research Centre
Noordwijk 2201 AZ, Netherlands

Alexander Hadjiivanov

European Space Technology and Research Centre
Noordwijk 2201 AZ, Netherlands

Jai Grover

European Space Technology and Research Centre
Noordwijk 2201 AZ, Netherlands

Gernot Heißel

European Space Technology and Research Centre
Noordwijk 2201 AZ, Netherlands

Yuri Shimane

School of Aerospace Engineering
Georgia Institute of Technology
Atlanta, Georgia 30332, United States of America

Chit Hong Yam

Mission Design and Operations Group, ispace inc.
Sumitomo Fudosan Hamacho Building 3F, 3-42-3
Nihonbashi Hamacho, Chuo-ku, Tokyo, Japan 103-0007

ABSTRACT

In 2023, the 12th edition of Global Trajectory Competition was organized around the problem referred to as “Sustainable Asteroid Mining”. This paper reports the developments that led to the solution proposed by ESA’s Advanced Concepts Team. Beyond the fact that the proposed approach failed to rank higher than fourth in the final competition leader-board, several innovative fundamental methodologies were developed which have a broader application. In particular, new methods based on machine learning as well as on manipulating the fundamental laws of astrodynamics were developed and able to fill with remarkable accuracy the gap between full low-thrust trajectories and their representation as impulsive Lambert transfers. A novel technique was devised to formulate the challenge of optimal subset selection from a repository of pre-existing optimal mining trajectories as an integer linear programming problem. Finally, the fundamental problem of searching for single optimal mining trajectories (mining and collecting all resources), albeit ignoring the possibility of having intra-ship collaboration and thus sub-optimal in the case of the GTOC12 problem, was efficiently solved by means of a novel search based on a look-ahead score and thus making sure to select asteroids that had chances to be re-visited later on.

Keywords GTOC · low-thrust · asteroid mining · machine learning · mixed-integer linear programming · nonlinear programming

Nomenclature

\mathbf{r}	spacecraft position vector (m)
\mathbf{v}	spacecraft velocity vector (m/s)
m	mass (kg)
$\mathbf{x} = [\mathbf{r}, \mathbf{v}]$	spacecraft state, containing position and velocity.
$\mathbf{y} = [\mathbf{x}, m]$	spacecraft state, containing position, velocity, and mass.
t	epochs (specific points in time)
T_{max}	maximum thrust (N)
T	time of flight along an asteroid transfer (s)
I_{sp}	specific impulse (s)
Δv	impulsive velocity changes (m/s)
\mathcal{S}	a collection of spacecraft (or ships)
σ	a spacecraft (or ship)
\mathcal{A}	the collection of (GTOC12) asteroids
α	an asteroid
a	acceleration (m/s^2)
\mathbf{v}, v	boldface symbols indicate vectors, the non boldface version indicates their norm.

1 Introduction

Global Trajectory Optimization Competitions (GTOC) [1] represent a biennial cornerstone event within the international aerospace community, dedicated to addressing the intricacies of interplanetary trajectory optimization. The 12th edition of this well established competition, held in June-July 2023, proposed a challenging design of a “sustainable asteroid mining” mission. The problem demanded the concurrent extraction of resources from a set \mathcal{A} of 60,000 target asteroids, to be accomplished during a fixed 15 years wide window (from 2035-Jan-01 to 2050-Jan-01) by multiple spacecraft. The participating spacecraft, dispatched from Earth and possibly flying by Venus and Mars, had to be meticulously designed to maximize the quantity of mined material returned to our home planet. A comprehensive exposition of the mathematical intricacies underpinning the problem definition can be found in [2], while in this paper we will primarily provide essential definitions and selectively reference these mathematical foundations. For the purpose of clarity, we shall employ the term ‘ship’ interchangeably with ‘spacecraft.’ In the context of the multi-spacecraft asteroid mining mission presented in GTOC12, each ship possesses the capability to deploy a specified number of mining devices onto the asteroids’ surface. Furthermore, these ships have the capacity to collect mined resources if a mining device is already in place on the visited asteroid. Importantly, each ship is not confined to gathering material exclusively from asteroids where it initially deposited a miner; it can collect resources from asteroids where miners were deployed by other ships. We introduce the concept of n -ship *ensemble*, defined by a set $\mathcal{S} := \{\sigma_i\}$ comprising ships capable of collectively visiting each asteroid precisely twice: once for miner deployment and once for resource collection. To uniquely indicate the asteroid visited by each ship, we represent it with an integer corresponding to the asteroid’s identification, that is, we consider the set of asteroids given in the competition as $\mathcal{A} \subseteq \mathbb{N}$, but will also silently identify an $\alpha \in \mathcal{A}$ with the corresponding celestial object and all its properties. As an illustrative example, a three-ship *ensemble* might be represented as follows:

$$\mathcal{S}_3 = \begin{cases} \sigma_1 = [12, 45, 33, 23, 45, 87] \\ \sigma_2 = [49, 9, 12, 84, 33, 23] \\ \sigma_3 = [13, 87, 49, 9, 84, 13] \end{cases}$$

while an example of a one-ship *ensemble* (which we will refer to also as a self-sufficient ship) is:

$$\mathcal{S}_1 = \{ \sigma_1 = [12, 45, 33, 97, 23, 23, 33, 97, 12, 45] \}$$

While the cooperative aspect of this mining problem (i.e. using high dimensional *ensembles*) is most interesting and eventually allows for mining and returning to Earth more mass, it also adds a great deal of complexity to the problem and relatively good missions can be obtained also using only self-sufficient ships. It is at this point necessary to mention

that all the top three teams in the GTOC 12 leaderboard made extensive use of large *ensembles* thus proving their worth and advantages. In this paper, instead, we will present the design of a mining mission that only considers self-sufficient ships (i.e. one-ship *ensembles*) as our attempts to leverage the collaborative aspect of the mining mission were never able to match the quality of the solution we found considering only the simpler case. The rest of the paper is structured as follows. In Section §2 we outline the overall strategy to design such a mission. In Section §3 we discuss the creation of low-thrust trajectory databases for the initial and last mission phases, i.e., coming from and returning to the Earth. In the following Section §4 we discuss the differences between low-thrust trajectory *hops* (i.e., transfers between asteroids) and their impulsive representation as Lambert’s arcs and present several innovative techniques developed to cancel such a gap. In Section §5.2 we discuss the search algorithm used to assemble, independently, self-sufficient ships. Finally, in Section §6 we discuss the construction of a multi-spacecraft mission collectively satisfying the imposed constraints and we conclude, in Section §7, describing our final design.

2 The Overall Strategy

Each ship, as detailed in the problem description, has a starting mass $m_0 \leq 3000$ kg, a dry mass $m_d = 500$ kg and can deliver a maximum thrust $T_{max} = 0.6$ N with a specific impulse $I_{sp} = 4000$ s. Each ship also carries I miners each with a mass $m_M = 40$ kg. Assuming an average ship with a propellant mass of $m_p = 2000$ kg, the straightforward application of the Tsiolkovsky rocket equation $\Delta V = -I_{sp}g_0 \log \frac{m_f}{m_i}$ returns, for such a ship, a maximum ΔV capability of roughly 43 km/s which is delivered, thrusting constantly at the maximum possible level, in around $t_{thrust} = I_{sp}g_0 \frac{m_f - m_i}{T_{max}} = 4.14$ years. It is thus evident that the available ships are very agile and capable of hopping between multiple asteroids. This is true also in view of the actual spatial density of the asteroids, reported in Figure 1, which suggests most of the good transfer opportunities between asteroids to be in the bracket [2.7, 2.9] AU and hence the ships to be mostly thrusting in that area where the Sun gravity is relatively weak. A mining mission may be thus divided into three phases which we designed separately and then connected:

1. Leaving the Earth: potentially utilizing Mars and Venus fly-bys, each spacecraft reaches a high-density region in the asteroid belt to maximize its opportunities to find favorable inter-asteroid transfers. Ideally, this trajectory should be designed early within the 15-year operational window to facilitate the commencement of mining operations and accumulate the largest possible quantity of material (with a defined mining rate of 10 kg/yr [2]).
2. Deploy and Mine: for spacecraft ensembles, an extensive search for sequences of low-thrust transfers between asteroids is performed to link the initial and final trajectory segments.
3. Returning to Earth: initiated as late as possible within the 15-year operational window and also potentially employing Mars and Venus fly-bys, return trajectories from the asteroids are crafted to allow the return of the maximum amount of mined resources.

In the process of developing our solutions during the competition, a significant portion of our achievements drew upon prior research. We provide a brief overview of these foundational elements. To devise the low-thrust trajectories and address optimal control challenges, our approach leaned on the integration of a direct approach, as outlined by Sims [3], in conjunction with the utilization of the Non-Linear Programming solver SNOPT [4]. This combination proved instrumental in addressing efficiently the needed trajectory optimization problems.

For the task of asteroid selection, a key component in ranking potential target asteroids, we employed the orbital metric approach [5]. This method, extensively tested and validated, was found to yield results consistent with the selections made by the winning trajectory in the GTOC11 competition [6]. In our efforts to construct machine-learning models for the solutions to the Optimal Control Problems, we relied strongly on the PyTorch library [7]. PyTorch provided a robust framework for developing and training these models, facilitating the integration of deep learning techniques into our approach. The PyKEP and PyGMO software packages were also indispensable for the implementation of fundamental astrodynamical routines and optimization methods [8]. These software tools streamlined the development of astrodynamics-related components within our solutions. Additionally, in solving the integer linear programming problems (ILPs) that arose during the asteroid selection phase, we leveraged the capabilities of the open-source SCIP optimization suite [9]. The combination of these tools and libraries enabled us to develop robust, data-driven solutions for various optimal control problems we defined (see next section) and other critical aspects of the competition.

3 Databases with Departure and Return Options

A large number of candidate trajectories to bring the spacecraft from the Earth to their first asteroid, as well as the final leg departing the last visited asteroid to return to Earth, were computed and stored as databases to be used in the subsequent search of the “deploy and mine” phase.

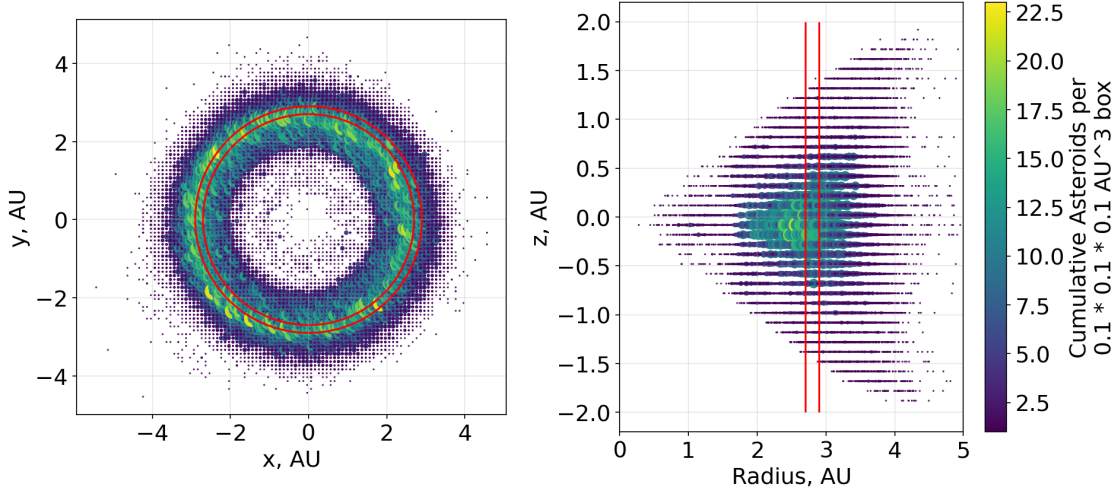


Figure 1: Spatial density of GTOC12 asteroids x - y plane (left) and in the radius- z plane (right), calculated by computing the asteroid positions at epochs 69807, 70107, and 70407 MJD corresponding to early mid and late mission epochs, and binning the Cartesian space with cubes of 0.1 AU size. Red lines show circular bounds between 2.7 and 2.9 AU.

Fly-bys with Venus or Mars have been under thorough consideration for both the initial and final legs of the trajectory. Extensive analysis has revealed that employing a Venus fly-by never offers any significant advantage over a direct transfer, primarily due to the fact that the majority of the GTOC12 asteroids are positioned beyond Earth's orbit. The use of a Mars fly-by, instead, may offer a substantial benefit, albeit only in rare cases. This is, for example, shown in Figure 2 where some optimal low-thrust transfers appear that use Mars fly-bys, but are outnumbered by similar opportunities not using Mars.

Overall, the relatively high departure and return V_∞ allowed (6 km/s) from and to Earth, makes direct transfers particularly beneficial. Furthermore, the utilization of a fly-by generally necessitates precise alignment and phasing of the planets involved and the target asteroid: given the GTOC12 mission's requirements, we have found gravity assists to be mostly detrimental or marginally helpful.

3.1 A Database of Departure Legs

For each asteroid α , we introduce and solve two distinct classes of optimal control problems, briefly described as follows:

$$\mathcal{P}_1 : \begin{cases} \min: & t_f \\ \text{subject to:} & m_f \geq m_{f \min} \\ & t_s \geq 64328 \text{ MJD} \\ & \dots \end{cases} \quad \mathcal{P}_2 : \begin{cases} \max: & m_f \\ \text{subject to:} & t_f \leq t_{f \max} \\ & t_s \geq 64328 \text{ MJD} \\ & \dots \end{cases} \quad (1)$$

where, $m_{f \min} = [2300, 2500, 2600]$, $t_{f \max} = 64328 + [570, 600, 650, 750]$ and direct, Venus, and Mars fly-by trajectory models are considered. The two optimal control problems classes reflect the desire to have both time optimal trajectories that are not using too much mass, and mass optimal trajectories not using too much time. The specific values used for $m_{f \min}$ and $t_{f \max}$ were tuned and finally chosen as we performed experiments during the competition. The modified Julian date of 64328 corresponds to the Gregorian date 2035-Jan-01, i.e. the start of the mission window. We also use the subscripts s, f to indicate the start and final conditions along the transfer and omit a formal description of all the constraints resulting from the dynamics, the boundary conditions, and the control constraints as they are not important in this context. We thus created $60,000 \times 7$ optimal control problems that were solved using a simplified direct transcription method based loosely on the well-established Sims-Flanagan approach [3]. For transfers involving fly-by at Venus or Mars, a pre-screening based on a single deep space manoeuvre (DSM) model [10] was conducted to prune for candidate asteroids that are well-phased with the planet in question.

The result of this departure leg search indicated that among the 60,000 asteroids available, only a subset of approximately 18,000 exhibited a favorable phasing and were consequently considered as potential initial targets. All the most promising optimal transfer options (i.e. non-dominated) were stored in a database $\mathcal{D}_{\text{dep}} \subseteq \mathcal{A} \times \mathbb{R} \times \mathbb{R}$ that contains an

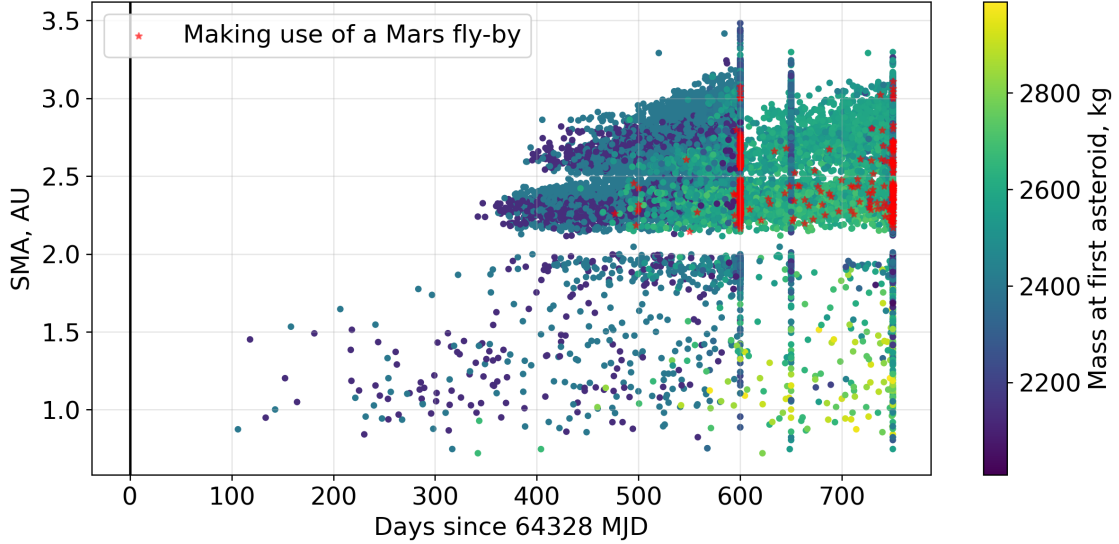


Figure 2: Visualization of the low-thrust transfers included in the departure database \mathcal{D}_{dep} . A total of 91,135 non-dominated transfers to 18,504 asteroids were included. The 665 transfers making use of a Mars fly-by are marked. The transfers hitting the bounds on $t_{f \text{ max}}$ are clearly visible as vertical lines.

element (α, t, m) if there is a departure leg that arrives at asteroid α at time t with a remaining mass of m . Figure 2 visualizes \mathcal{D}_{dep} . Only 665 transfers in this non-dominated set made use of a Mars fly-by, and none used Venus.

3.2 A Database of Return Legs

As to compute a number of possible return options, for each asteroid α , we introduce the following optimal control problem:

$$\mathcal{P}_3 : \begin{cases} \max: & m_f \\ \text{subject to:} & t_s \geq 69807 - \Delta t_{\text{max}} \\ & t_f \leq 69807 \\ & \dots \end{cases} \quad (2)$$

The modified Julian date 69807 corresponds to the Gregorian date 2050-Jan-01, i.e., the end of the mission window. In essence, we compute the maximum amount of mined material that can be returned to Earth from each asteroid assuming some initial mass m_s and to depart not earlier than Δt_{max} days from the end of the mission window. For favorable return options, this value is expected to decrease, potentially in a nonlinear fashion, as Δt_{max} increases, signifying a gradual loss of asteroid-Earth phasing. We have solved this optimal control problem for a range of Δt_{max} values, specifically $\Delta t_{\text{max}} = 800, 750, 700, 650, 550, 500$ days. Although we initially considered various departure mass values m_s , our preliminary findings consistently indicated that the ratio m_f/m_s (i.e., the required Δv) remained relatively constant for a given asteroid. Consequently, we opted to focus exclusively on one value, namely $m_s = 1200$ kg, for the construction of the return database. Formally, the database $\mathcal{D}_{\text{ret}} \subseteq \mathcal{A} \times \mathbb{R} \times \mathbb{R}$ contains, as the departure database, triplets (α, t, m) indicated that a spacecraft of mass m on an asteroid α at time t can return to Earth (no gravity assists options were found that helped returning more mass to the Earth.). The entries within the return databases are depicted in Figure 3.

4 Filling the Gap Between Impulsive and Low-thrust Solutions

To allow for the efficient design of multiple asteroid rendezvous missions utilizing a purely impulsive model, it is imperative to comprehend the difference with its low-thrust counterpart. Using the impulsive Δv to extract an estimation of the actual propellant mass to be used is a widely employed method, but also one well-known to lead to sub-optimal designs. On many occasions, a given transfer might not be feasible at all in low-thrust, since the spacecraft's initial mass, or the desired time of flight, might be too constraining to enable the transfer. We thus developed several approximations to have a good understanding of whether a certain given spacecraft's initial mass is sufficient to make a fixed-time transfer. We then leveraged the Lambert solution and developed analytical and machine learning (ML)-based

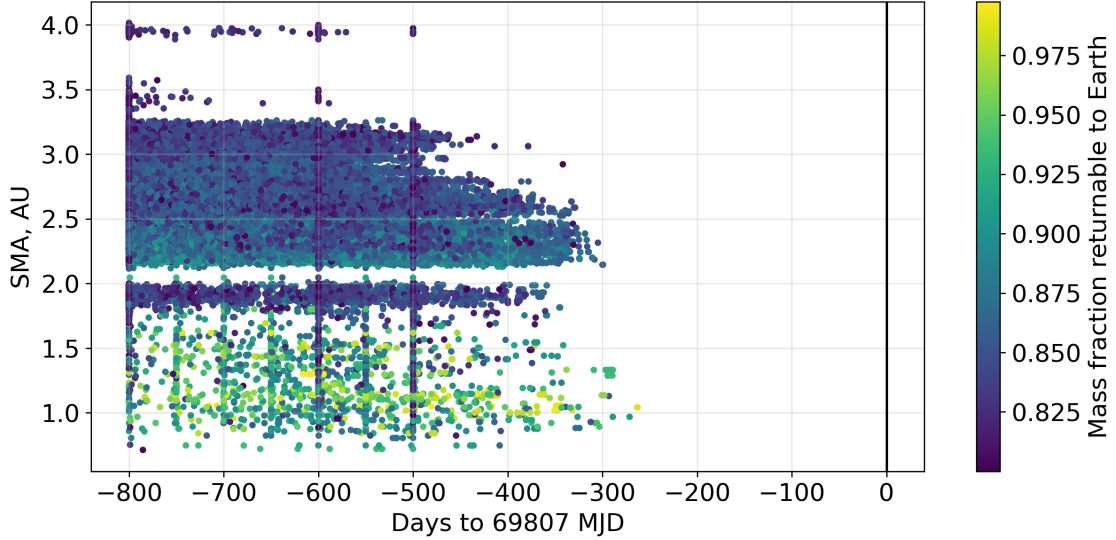


Figure 3: Departure epoch vs semi-major axes for all entries in the return database D_{ret} , consisting of 190,976 transfers to 59,993 asteroids.

approximations that helped us to accurately transition from the high to the low-thrust world, without directly solving an optimal control problem.

4.1 MIM and MINT: the Maximum Initial Mass and the Minimum Time-of-flight

Let us consider a rendezvous trajectory between two asteroids α_s and let α_f , t_s , and t_f be the starting and arrival epochs of the spacecraft at the two asteroids. In correspondence to such a fixed time of flight, there will be one well-defined transfer maximizing the initial spacecraft mass. This transfer corresponds to a trajectory with no coast arcs since if a coast arc was present in the optimal solution, it would be possible to have an infinitesimally larger initial mass, contradicting the optimality assumption. The optimal control problem defining the maximum initial mass m^* can be formally stated as:

$$\mathcal{P}_{\text{MIM}} : \left\{ \begin{array}{l} \text{given: } \alpha_s, \alpha_f, t_s, t_f \\ \text{find: } \mathbf{u}(t) \\ \text{to maximize: } m_s \\ \text{subject to: } \mathbf{x}(t_s) - \mathbf{x}_{\alpha_s}(t_s) = \mathbf{0} \text{ ,} \\ \mathbf{x}(t_f) - \mathbf{x}_{\alpha_f}(t_f) = \mathbf{0} \\ \dot{\mathbf{y}} = \mathbf{f}(\mathbf{y}, \mathbf{u}) \\ |\mathbf{u}| \leq T_{\text{max}} \end{array} \right. \quad (3)$$

where \mathbf{x} indicates the state (e.g., a six-dimensional vector expressing the position and velocity in Cartesian coordinates), $\mathbf{y} = [\mathbf{x}, m]^T$ indicates the state augmented with the mass, the subscripts α indicate the asteroids and \mathbf{f} indicates the spacecraft controlled dynamics. If the initial spacecraft mass were to be higher than the maximum initial mass $m_s > m_s^*$, then the transfer, also referred to as a *hop*, cannot be performed in low-thrust (i.e., the spacecraft is said to be “fat” as it weighs too much to be able to perform the hop). The optimal control problem shown in Eq. (3) can be solved by varying t_f : the resulting optimal starting mass m_s will be a continuous curve starting from the origin since to perform a hop with an infinitesimal time of flight an infinitesimally small mass is needed. In Fig. 4, we show an example of such a curve computed solving accurately the corresponding optimal control problems for six different transfers between asteroids of the GTOC12 database corresponding to randomly selected t_s values. Given a point on the curve, when the spacecraft’s initial mass is below that value, the spacecraft is said to be slim and the transfer is feasible, otherwise, the spacecraft is fat and the transfer is not feasible.

One may now ask the dual question: given an assigned starting mass m_s , what is the minimum time of flight our spacecraft can rendezvous with the destination asteroid? The answer indicated with t_f^* and called MINT, is

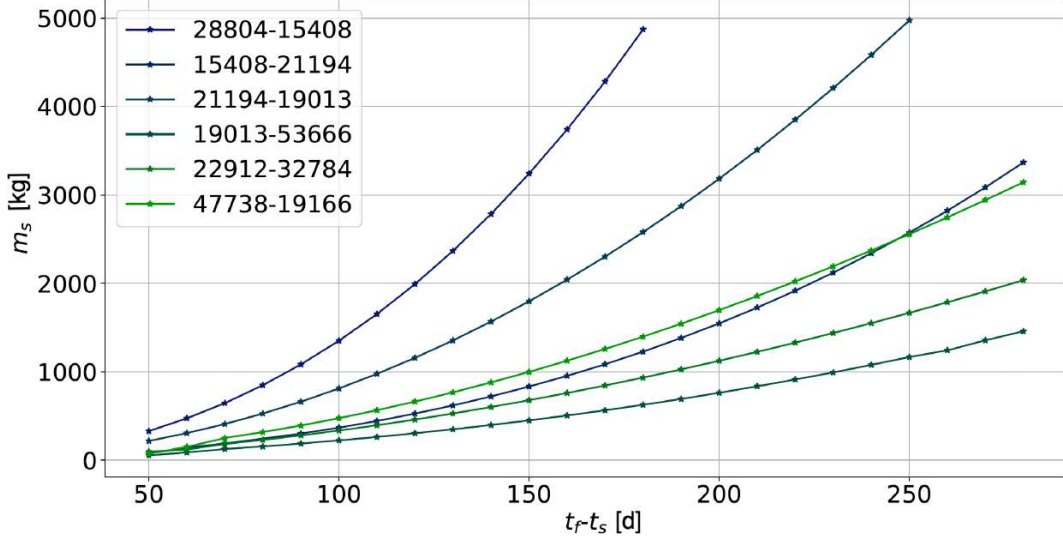


Figure 4: Maximum initial mass curve as a function of time from the start of the mission for different asteroid hops. In the legend, we display the database ID of the departing and arriving asteroids.

mathematically the solution of the following optimal control problem:

$$\mathcal{P}_{\text{MINT}} : \begin{cases} \text{given: } \alpha_s, \alpha_f, t_s, m_s \\ \text{find: } \mathbf{u}(t) \\ \text{to minimize: } t_f \\ \text{subject to: } \mathbf{x}(t_s) - \mathbf{x}_{\alpha_s}(t_s) = \mathbf{0} , \\ \mathbf{x}(t_f) - \mathbf{x}_{\alpha_f}(t_f) = \mathbf{0} \\ \dot{\mathbf{y}} = \mathbf{f}(\mathbf{y}, \mathbf{u}) \\ |\mathbf{u}| \leq T_{\max} \end{cases} \quad (4)$$

To solve this problem, one may simply invert the curve $m_s^*(t_f)$ into $t_f^*(m_s)$, thus finding the intersection of a horizontal fixed mass line with the plot in Figure 4. Computing the MIM and MINT from their definitions as solutions to optimal control problems is computationally demanding and is likely to be not useful. Hence, we propose a few fast approximators, considering that for the problem of interest, we can expect most thrust arcs to happen in less than a complete revolution.

4.2 Analytical Approximations

Consider the low-thrust transfer from α_s at epoch t_s to α_f at epoch t_f . As a naive approximation for the maximum initial mass m^* , we can compute a total Δv solving the Lambert problem with transfer time T and summing the two resulting velocity discrepancies. One can then set:

$$m^* \approx \frac{T_{\max} T}{\Delta v}, \quad (5)$$

However, this approximation is not very accurate. The maximum initial mass approximation (MIMA) was developed with the idea of improving the above formula with a more sensible approximation [5]. To derive it, the motion of the spacecraft traveling from α_s to α_f is described as a variation with respect to a corresponding Lambert transfer defined by the two velocity impulses. It is assumed that the spacecraft is subject to a piecewise constant acceleration (both in magnitude and direction): this configuration, at the basis of the original developments to derive the MIMA summarized here, is depicted in Figure 5. By imposing that the two accelerations are equal in magnitude and that they need to provide a total velocity change that corresponds to the Lambert cost, the problem can be formulated and solved to obtain the expression for the thrust magnitudes and directions, as well as the switching time. This results in the following approximation for the maximum initial mass [5]:

$$m_{\text{MIMA}}^* = 2 \frac{T_{\max}}{a_D} \left(1 + \exp\left(\frac{-a_D T}{I_{sp} g_0}\right) \right)^{-1}, \quad (6)$$

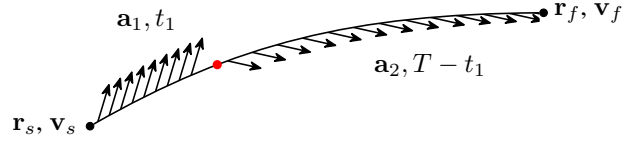


Figure 5: To approximate the maximum initial mass (MIM) we find an analytical representation for a low-thrust transfer that employs a piecewise constant thrust. All variables $\mathbf{a}_1, \mathbf{a}_2, t_1$ can be found expanding the solution around the corresponding Lambert problem (i.e. a ballistic transfer from \mathbf{r}_s to \mathbf{r}_f in T).

where T is the time of flight, and a_D is the magnitude of the acceleration of each of the two segments.

While MIMA is quick to calculate and provides a much better estimation of the feasibility of the jump compared to the naive approach, it still represents an idealized and impractical transfer that does not accurately represent reality. We thus developed a second approximation (aptly named MIMA2) incorporating first-order information about the trajectory. The derivation starts with the same spirit as for MIMA and is summarized below. The spacecraft state $\mathbf{x}_K = [\mathbf{r}_K, \mathbf{v}_K]^\top \in \mathbb{R}^6$ along a ballistic arc connecting the positions of two asteroids in the time T is the solution to the (Keplerian) differential equation:

$$\dot{\mathbf{x}}_K = \mathbf{F}(\mathbf{x}_K) \quad (7)$$

where $\mathbf{F} = [\mathbf{v}_K, -\mu\mathbf{r}_K/r_K^3]^\top$. Executing this ballistic transfer requires a ship to perform two impulsive maneuvers, denoted as $\Delta\mathbf{v}_s$ and $\Delta\mathbf{v}_f$, at the initiation and conclusion of the arc. The magnitudes of these maneuvers are readily calculated to align the departure and arrival orbital velocities with those along the ballistic arc, which is determined as a solution to the Lambert problem [11].

Consider the spacecraft dynamics under the effect of a finite thrust. The equations of motion become:

$$\dot{\mathbf{x}} = \mathbf{F}(\mathbf{x}) + \tilde{\mathbf{a}}(t) \quad (8)$$

with $\tilde{\mathbf{a}}(t) = [\mathbf{0}, \mathbf{a}(t)]^\top$ and where $\mathbf{a}(t)$ is the additional, low-thrust induced, acceleration. We write the spacecraft motion, during the low-thrust transfer between two asteroids, as a perturbed Keplerian arc and thus write $\mathbf{x} = \mathbf{x}_K + \delta\mathbf{x}$. Substituting this into Eq. (8), Taylor approximating \mathbf{F} to first order around \mathbf{x}_K and using Eq. (7) yields

$$\delta\dot{\mathbf{x}} = \mathbf{F}'(\mathbf{x}_K)\delta\mathbf{x} + \tilde{\mathbf{a}}(t) \quad (9)$$

describing the dynamics of the perturbation vector. The rendezvous conditions with α_s and α_f are enforced by imposing the boundary conditions $\delta\mathbf{x}(0) = \delta\mathbf{x}_0 = [\mathbf{0}, -\Delta\mathbf{v}_s]^\top$, $\delta\mathbf{x}(T) = \delta\mathbf{x}_T = [\mathbf{0}, \Delta\mathbf{v}_f]^\top$, where here and in the following a subscript on $\delta\mathbf{x}$ denotes the evaluation of that quantity at a specific time. The homogeneous equation (i.e. Eq. (9) with $\tilde{\mathbf{a}} = \mathbf{0}$) admits the general solution $\delta\mathbf{x}(t) = \mathbf{M}(t)\delta\mathbf{x}_0$, where $\mathbf{M}(t)$ is the state transition matrix. We use the variation of parameters technique (see e.g. [12]) to solve the inhomogeneous equation, hence we consider \mathbf{x}_0 as a time-varying quantity, change its symbol to $\mathbf{z}(t)$ and write the solution as $\delta\mathbf{x}(t) = \mathbf{M}(t)\mathbf{z}(t)$. Substituting this expression back into Eq.(9), after simplification, we obtain the differential equation for $\mathbf{z}(t)$:

$$\dot{\mathbf{z}} = \mathbf{M}^{-1}(t)\tilde{\mathbf{a}}(t) \quad (10)$$

Equation (10) is an ordinary differential equation for which we can explicitly write the solution at the time T as:

$$\delta\mathbf{z}_T = \delta\mathbf{z}_0 + \int_0^T \mathbf{M}^{-1}(s)\tilde{\mathbf{a}}(s) ds$$

which, accounting for the definition of $\mathbf{z}(t)$ and the identity $\mathbf{M}_0 = \mathbf{I}$, becomes:

$$\delta\mathbf{x}_T = \mathbf{M}_T\delta\mathbf{x}_0 + \mathbf{M}_T \int_0^T \mathbf{M}^{-1}(s)\tilde{\mathbf{a}}(s) ds \quad (11)$$

Note how the only unknown in this equation is the acceleration profile $\tilde{\mathbf{a}}(t)$.

We now assume, similarly to what is done in the case of the MIMA derivation, that the low-thrust transfer is made of two constant thrust arcs $\mathbf{a}_1, \mathbf{a}_2$ of duration t_1 and $T - t_1$. Approximating the resulting two integrals on the right-hand side of Eq. (11) by Simpson's rule we obtain,

$$\delta\mathbf{x}_T - \mathbf{M}_T\delta\mathbf{x}_0 = \frac{\mathbf{M}_T}{6} \left(\left(\mathbf{M}_0^{-1} + 4\mathbf{M}_{t_1/2}^{-1} + \mathbf{M}_{t_1}^{-1} \right) \Delta\mathbf{v}_1^* + \left(\mathbf{M}_{T-t_2}^{-1} + 4\mathbf{M}_{T-t_2/2}^{-1} + \mathbf{M}_T^{-1} \right) \Delta\mathbf{v}_2^* \right) \quad (12)$$

where $\Delta \mathbf{v}_1^* = [\mathbf{0}, \mathbf{a}_1 t_1]^\top$, $\Delta \mathbf{v}_2^* = [\mathbf{0}, \mathbf{a}_2 (T - t_1)]^\top$ and where for later convenience we substitute t_2 for $T - t_1$ in the subscripts of the second Simpson approximation.

Given a choice for the switching time t_1 , the above system of equations admits only one solution in the unknowns $\Delta \mathbf{v}_1^*$ and $\Delta \mathbf{v}_2^*$ which only appear linearly. This corresponds to the fact that there is only a unique solution to satisfy the boundary conditions when we force the thrust structure into this two-segment piecewise-constant thrust law. We choose the switching time t_1 by demanding that the magnitude of the two accelerations be equal and thus solving the equation

$$(T - t_1) |\Delta \mathbf{v}_1^*| = t_1 |\Delta \mathbf{v}_2^*| \quad (13)$$

iteratively for t_1 . We have thus found an approximation for a continuous thrust trajectory that is able to transfer between two generic asteroids in the time T using two constant-thrust segments. An approximation that can be computed at the cost of evaluating the state transition matrix \mathbf{M} at a few points along the ballistic transfer!

Such a trajectory is a good approximation for the optimal low-thrust transfer that typically results in solving the corresponding optimal control problem for the maximum initial mass. We thus compute the necessary acceleration from

$$a = |\mathbf{a}_1| = |\mathbf{a}_2| = \frac{|\Delta \mathbf{v}_1^*|}{t_1} = \frac{|\Delta \mathbf{v}_2^*|}{T - t_1} \quad (14)$$

and approximate the maximum initial mass via the equation:

$$m_{\text{MIMA2}}^* = \frac{T_{\text{max}}}{a}. \quad (15)$$

In Figure 6, we display the error expressed as the difference between the maximum initial mass of the solution of the optimal control problem and the approximated one, using either MIMA or MIMA2 over around 400,000 low-thrust transfers with maximum initial masses within 700 and 3,000 kg. As we observe, MIMA2 has usually smaller errors than MIMA, although its average errors are slightly skewed towards the positive x-axis. Moreover, about 58.34% of the MIMA2 errors fall within the [-50,50] kg range, while this number drops to 53.00% for the MIMA.

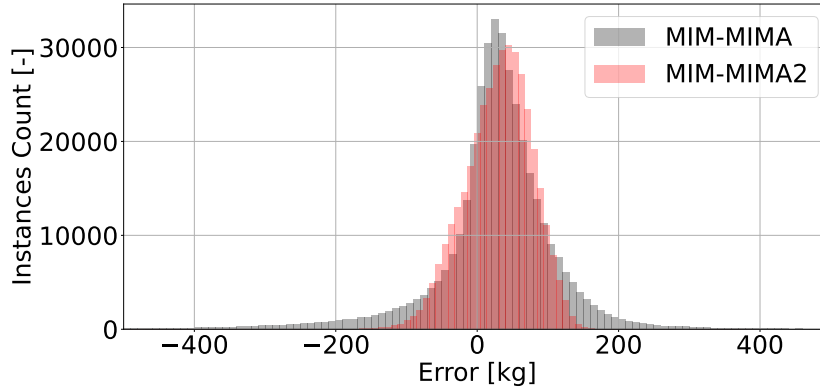


Figure 6: Difference in kilograms between MIM and MIMA, MIMA2 approximations.

The total required Δv can also be approximated for the MIM-MINT transfer using $\Delta v = |\Delta \mathbf{v}_1^*| + |\Delta \mathbf{v}_2^*|$. In cases where a spacecraft has a mass m_s lower than m_{MIMA2}^* , and optimally transfers in T between the two asteroids, there will be a coasting arc and a lower Δv requirement. In that situation Eq.(12) is still valid, but the durations of the thrust arcs, t_1 and t_2 , are both unknown as they no longer sum up to T . Since we are assuming to know the starting mass, though, we may also assume $a = \frac{T_{\text{max}}}{m_s}$. Thus, we solve the system $\{|\Delta \mathbf{v}_1^*| = t_1 a, |\Delta \mathbf{v}_2^*| = t_2 a\}$ for t_1 and t_2 , and approximate the total Δv needed for a generic hop, i.e. one that also has a coast arc.

As already discussed in Section 4.1, the maximum initial mass and minimum time of flight are closely related concepts. Using a root solver, one can derive from MIMA and MIMA2, the corresponding approximated minimum time of flights MINTA and MINTA2.

4.3 Machine Learning Approximations

During the competition, a vast amount of optimal control problems of rendezvous transfers among pairs of asteroids were solved (e.g., to check the validity of the provided approximations). Therefore, it quickly became apparent that

supervised machine learning approaches could be used to try and find ML-based approximations of the minimum fuel required for the hop in the low-thrust world. We constructed a database of about 800,000 transfers, which were found by solving the low-thrust fuel-optimal control problem and we trained a supervised neural network to predict the ratio between the final and initial mass (which is directly related to the propellant cost of the transfer, via the Tsiolkovsky equation). The objective was, given a rendezvous transfer between two asteroids, with fixed initial and final time (and therefore time of flight) and fixed initial mass, to find the minimum propellant required by the transfer.

We used a feed-forward neural network with two hidden layers and 50 nodes per layer. As attributes we included the cost of the Lambert transfer between the two asteroids as well as the time of flight, the initial mass, the difference of their eccentricities, mean motions, and the semi-major axis. A main concern was to ensure that the network treated equally hops between asteroids that were at the same distance from the Sun and were defined by the same transfer geometry. To achieve this, instead of feeding as attributes to the network the position and velocity of the two asteroids in the inertial frame, we used the relative position and velocity and we additionally expressed their coordinates as spherical coordinates in the LHLV frame (Local Horizontal Local Vertical) attached to the departure asteroid. Furthermore, we also used as attributes both the impulsive velocity vectors derived from the difference of velocity between the Lambert arc solution and the asteroids' velocity (this corresponds to the velocity vectors needed to perform the Lambert transfer that enables the rendezvous). These represent a fast and informative guess of the solution and were found to greatly improve the results. Both were also expressed using the spherical coordinates with respect to the same reference frame as the relative position and velocity. In Figure 7, we display a schematic representation of the neural network architecture and inputs/outputs used in the competition.

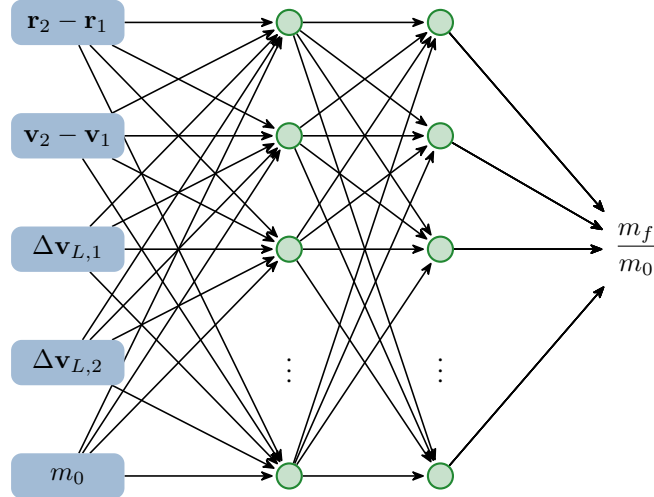


Figure 7: Schematic representation of neural network architecture used to learn the low-thrust transfer cost. Vectors are all expressed in spherical coordinates in the orbital frame of the departure body to ensure rotational symmetry.

Finally, all the attributes, together with the initial mass and time of flight, were normalized. We trained the network for 150 epochs, using a batch size of 1024 and a learning rate of 0.001. In Figure 8a, we show the results of the ML approximation compared to the analytical approximation across the 800,000 transfers in terms of absolute error (in kg) of the predicted mass, compared to the fuel-optimal control problem solution.

As we can see, for errors below around 800 grams in the final mass, the analytical approximation has the upper hand on the ML approximations. However, and most importantly, above 800 grams of absolute errors, the neural network manages to significantly reduce the errors (e.g. for more than 95% of the transfers the errors are kept below 10 kg on the final mass). Furthermore, the analytical approximation can have large errors up to 100 kg and would have dire consequences in any search strategy, causing substantial miscalculations on the propellant cost and the overall chain quality. Furthermore, the inference speed to predict from a hop and an initial mass the final mass is estimated to be about $\times 1.8$ faster for the ML approximator than for the analytical one. Due to the quality and speed of the results, we decided to employ the ML-based approximator to estimate the final mass (and hence the propellant cost) during the tree searches. For a comprehensive evaluation of the performance of various implemented approximations, we present in Figure 8b the mass errors incurred during a sequence of asteroid hops across diverse self-sustaining spacecraft. Specifically, we analyze 20 ships that made it to our final solution, which will be discussed in detail in Section 7. Each spacecraft undertakes between 16 and 20 hops: we show the error made in the mass computations along the full trajectory using distinct approximators: Lambert approximation, MINTA2-derived approximation, and

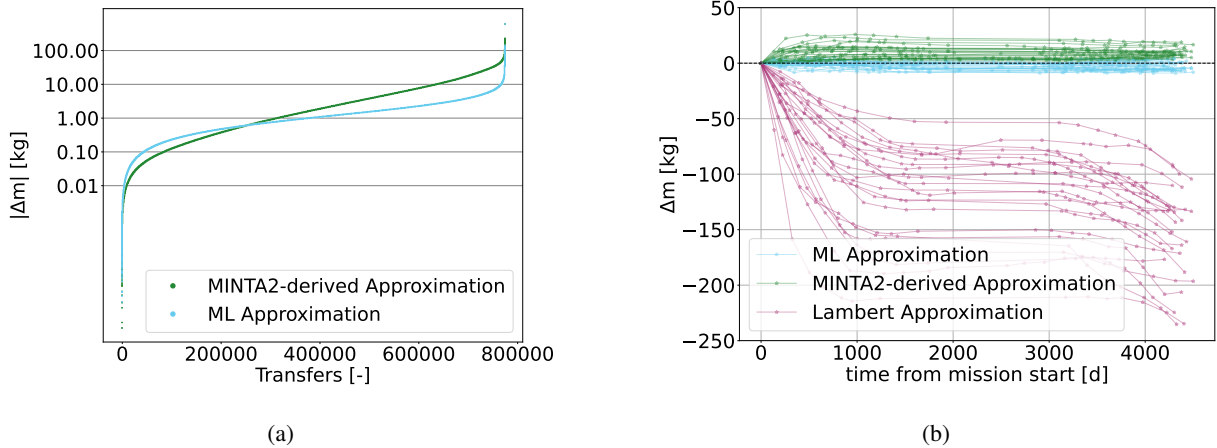


Figure 8: *Left*: Number of low-thrust optimal transfers approximated within some error using the MINTA2-derived and the analytical approximations. *Right*: Mass error accumulated along the time of flight by 20 different self-sufficient ships when the mass is approximated using Lambert, ML-based approximation and MINTA2-derived approximation.

ML approximation. Notably, the ML approximation applied to approximately 20 spacecraft, exhibits cumulative error values below 10-15 kg even after more than 15 hops. Similarly, the MINTA2-derived one shows marginally higher error values, reaching up to approximately 25 kg. In contrast, the Lambert approximation yields errors as substantial as 240 kg. Interestingly, the errors in Lambert approximations tend to escalate more prominently in the initial hops, while displaying a more stabilized behavior in subsequent hops. It is essential to note that this observation does not establish a general pattern for all asteroid hop sequences. However, it suggests that the combinatorial algorithm generating these solutions prioritizes time optimality in the initial hops and leans towards mass optimality in the later. In fact, the Lambert solution is expected to exhibit poor performance, especially closer to time optimality.

5 Design of Self-sufficient Ships

An ensemble is here defined as a collection of ships that visit asteroids in such a way that no asteroid is visited more than twice. One ship ensembles, here also called self-sufficient ships, are sub-optimal for this problem but offer some distinct advantages in general, and is what we ended up designing. The search for suitable trajectories for isolated ships can be massively parallelised without the need for synchronisation. In addition, it becomes simpler to manage the overall ensemble since any asteroid visited *once* (for miner deployment) can be simply put in a set of asteroids that are out of limits to all other ships. The flip side is that if the search is executed in parallel, it becomes necessary to devise a method to compile the final solution in order to ensure that the chosen ships have not visited the same asteroid by chance. We have developed and used two different search strategies to design self-sufficient ships, two approaches we call “Trajectory scaffolding” and a “A Beam Search that Looks Ahead in Time”.

5.1 Trajectory Scaffolding

This approach is based on the observation that a ship deploying a miner on an asteroid can remain in the same orbit as the asteroid without expending any fuel – referred to as ‘coasting’ – until some suitable point in the future when it can collect the material and return to Earth. Keeping in mind the fact that performing these manoeuvres (deployment, coasting, and retrieval) only *once* is wasteful, we concentrate on finding a sequence of efficient trajectories (Asteroid1 – Asteroid2 – Asteroid1, i.e., $\alpha_1, \alpha_2, \alpha_1$) that maximise the returned material; this corresponds to maximising the coasting time as mining time is directly proportional to the amount of mined material. We refer to this type of trajectory as a scaffold.

Let us denote an initial scaffolding manoeuvre to the i^{th} asteroid (Earth – α_i – Earth) as $E \rightarrow \alpha_i \rightarrow E$. A ship would be able to perform the manoeuvre and return to Earth with most of its propellant unused. Combining this with the long coasting time provides the ship with the opportunity to perform another scaffolding manoeuvre from α_i to another asteroid (α_j). Provided that the ship can return from α_j back to α_i *before* the departure time for the leg $\alpha_i \rightarrow E$, the ship would be able to collect as much material as has been mined during the coasting time at α_i as well as the material

mined from α_j . Then, from α_j the ship can perform another detour to another asteroid α_k and so forth, building a series of round trips – a *scaffold* – that has the original $E \rightarrow \alpha_i \rightarrow E$ round trip as a common base (Fig. 9).

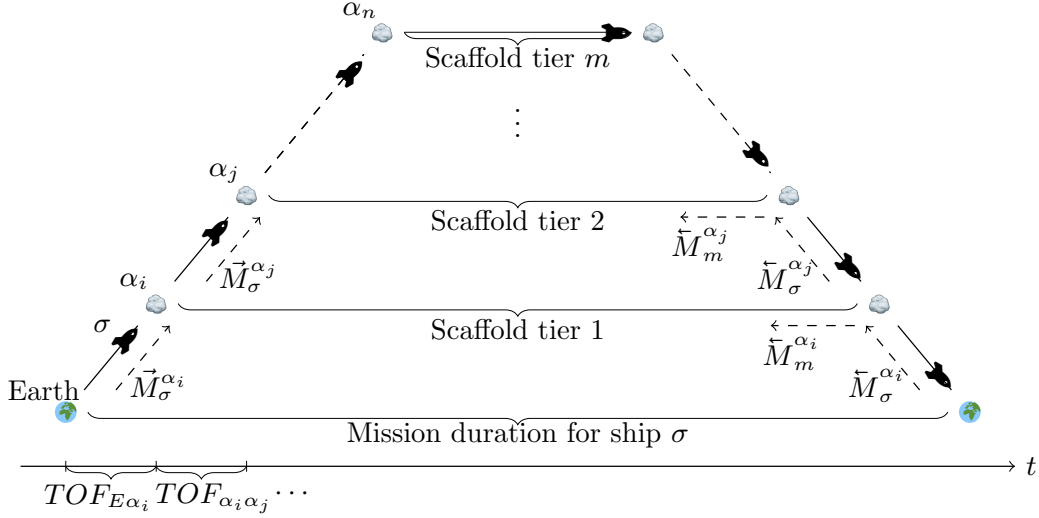


Figure 9: Illustration of the trajectory scaffolding approach. Here, $\alpha_{(\cdot)}$ indicates an asteroid, σ indicates a ship, and \vec{M}_σ and \overleftarrow{M}_σ denote the total mass of ship σ for the forward and backward legs, respectively. The mass estimate for the backward leg is required in order to estimate the time of flight (ToF) for each forward and backward leg with the MINT approximator. Refer to the text for details.

5.1.1 Building a Scaffold

As with all search strategies considered here, when building a scaffold, a ship should arrive from Earth as early as possible and leave back for Earth as late as possible in order to maximise the mining time. In addition, the symmetric nature of the round trip imposes the additional requirement that for each tier $\alpha_i \rightarrow \alpha_j \rightarrow \alpha_i$ in the scaffold, a feasible return hop can be made from α_j to α_i *before* the scheduled departure time for the hop $\alpha_i \rightarrow E$. The set of detour candidates \mathcal{A}_j are those asteroids that are reasonably close to the current asteroid α_i at both arrival and departure time. We use the orbital indicator [5, 13] to find suitable asteroids for detours.

The first tier of the scaffold is built by selecting an initial asteroid α_i and choosing the forward hop from Earth to the asteroid ($E \rightarrow \alpha_i$) and the hop back to Earth ($\alpha_i \rightarrow E$). These hops are chosen from among the options in the databases of arrival and return hops developed during the competition. The time of flight (ToF) for each hop (forward or backward) is assumed to be the minimum time of flight (MINT) as approximated by our MINTA2 approximator (see §4.2), with an added slack of 10 days to avoid solutions that are too aggressive in time optimality. Ultimately, the goal is to maximise the coasting window at the next detour (which is equivalent to minimising the TOF) while also minimising ΔV . However, there is one additional detail: while we know the mass of the ship for the forward hop, we must estimate the starting mass for the backward hop as this is required to estimate the MINT for the return hop.

The naïve way to estimate the mass of the ship for the backward hop is to subtract the fuel consumed during the forward hop, the mass of a miner, and an amount of material proportional to the coasting time. This can be done because once the ship has arrived at the new asteroid, it is assumed to be coasting without expending any fuel. However, this estimate is in fact quite inaccurate since presumably the ship would be performing multiple detours, thus expending more fuel and accumulating more material along the way, and therefore the actual mass at the end of all detours would look very different from this naïve approach.

Therefore, it is necessary to estimate the mass of the ship at each backward hop (Fig. 9). Assuming that the ship is currently at asteroid α_i , the backward mass $\overleftarrow{M}_\sigma^{\alpha_i}$ is estimated as follows based on the current amounts of fuel and material on board:

$$\overleftarrow{M}_\sigma^{\alpha_i} = \vec{M}_\sigma^{\alpha_i} - \frac{M_f}{2} + M_m^{\alpha_i} \quad (16)$$

Listing 1: Algorithm for building a trajectory scaffold \mathcal{S} for a single ship σ . Here, C denotes a chain of transfers that constitute a scaffold. Here, α_i is the first asteroid $M_{DB}^{\alpha_i}$ denotes the mass of the ship at the moment of arrival at asteroid α_i , and $t_{in}^{\alpha_i}$ and $t_{out}^{\alpha_i}$ denote the times of arrival at and departure from the current asteroid α_i . The current forward mass and the estimated backward mass of the ship σ are denoted as \vec{M}_σ and \overleftarrow{M}_σ , respectively. M_d denotes the dry mass of the ship, and $M_m^{\alpha(\cdot)}$ denotes the material collected from asteroid $\alpha(\cdot)$. S denotes the slack (in days) added to the ToF for each hop.

```

1  algorithm scaffold( $\alpha_i, M_{DB}^{\alpha_i}, t_{in}^{\alpha_i}, t_{out}^{\alpha_i}, ToF_{min} = 30, ToF_{max} = 250, S = 10$ )
2     $C \leftarrow []$  // Chain of scaffolding tiers (excluding hops from and to Earth, which are bootstrapped)
3     $\alpha, t_{in}, t_{out}, \vec{M}_\sigma \leftarrow \alpha_i, t_{in}^{\alpha_i}, t_{out}^{\alpha_i}, M_{DB}^{\alpha_i}$ 
4    while  $t_{in} < t_{out}$  do
5       $FW \leftarrow$  Top 500 closest asteroids to  $\alpha$  at time  $t_{in}$  // Forward transfer candidates
6       $BK \leftarrow$  Top 500 closest asteroids to  $\alpha$  at time  $t_{out}$  // Backward transfer candidates
7       $\mathcal{A}_j = FW \cap BK$  // Keep asteroids that are in both sets
8      for each  $\alpha_j \in \mathcal{A}_j$ 
9        for  $ToF \in (ToF_{min}, ToF_{max})$  // Partition the ToF
10       if (forward) // Mass for the forward hop
11          $M_\sigma \leftarrow \vec{M}_\sigma$ 
12       else // Mass for the backward hop
13          $M_\sigma \leftarrow \frac{\vec{M}_\sigma + M_d}{2} + M_m^{\alpha_i}$ 
14          $\rho_M^\alpha \leftarrow Mfm0(M_\sigma, \alpha, t_{in}, t_{out})$ 
15         if ( $M_\sigma < MIMA(\alpha, t_{in}, t_{in} + ToF)$  and  $0.5 < \rho_M^\alpha < 1$ )
16            $\vec{M}_\sigma \leftarrow \rho_M^\alpha \vec{M}_\sigma - 40$  kg // Depositing a miner reduces the mass by 40 kg
17            $\alpha \leftarrow \alpha_j$ 
18           if (forward) // Add the TOF to the time of arrival at  $\alpha_i$ 
19              $t_{in} \leftarrow t_{in} + ToF + S$ 
20           else // Subtract the TOF from the time of departure from  $\alpha_i$ 
21              $t_{out} \leftarrow t_{out} - ToF - S$ 
22           Append hops [ $\alpha_i \rightarrow \alpha_j$  and  $\alpha_j \rightarrow \alpha_i$ ] to  $C$ 
23           break
24  return  $C$ 

```

Here, $M_\sigma^{\alpha_i}$ indicates the total current mass of the ship, $M_f = \vec{M}_\sigma^{\alpha_i} - M_d$ is the mass of the fuel and any miners onboard (M_d is the dry mass of the ship, fixed at 500 kg), and $M_m^{\alpha_i}$ and $M_m^{\alpha_j}$ are the amounts of material collected at asteroids α_i and α_j , respectively. This estimate assumes that the ship can perform all future detours and return to the current asteroid with half of its remaining fuel, and allows us to determine the feasibility and the ToF for a backward transfer. Note that since we do not know in advance how many detours the ship would be able to make, M_f also includes the mass of an undetermined number of miners onboard.

For each new detour, ToFs in the range (30, 250) d are tested for feasibility¹ by checking if the current mass is below the approximated MIM (Eq. 6) for the respective ToF. A fixed buffer of 10 days is added to avoid transfers that were too aggressive and to absorb errors resulting from the ML approximators and the fact that the mass of miners is included in the total estimate of the fuel mass. If the trajectory is feasible, the ratio of the ship's mass after and before the hop is obtained from the ML-based approximator:

$$\vec{M}_\sigma^{\alpha_j} := \rho_M^{ij} \vec{M}_\sigma^{\alpha_i} \quad (17)$$

Here, ρ_M^{ij} denotes the ratio of the final to initial mass ($\frac{m_f}{m_0}$; cf. Fig. 7) for the transfer from asteroid α_i to asteroid α_j . An additional check ensures that $\rho_M \in (0.5, 1)$ to avoid exceedingly inefficient transfers (cases where $\rho_M \leq 0.5$) and erroneous outputs from the ML approximator (cases where $\rho_M \geq 1$). If the checks pass, ρ_M is used to compute the mass after the forward hop. This procedure is then repeated with the new asteroid α_j as the top tier of the scaffold until no feasible detour can be found. A detour is deemed infeasible when the departure time from the new detour candidate is evaluated to be *before* the arrival time at that candidate, a contradiction. The algorithm for building a trajectory scaffold in this way is given in Listing 1.

¹Naturally, the TOF for the backward hops is *subtracted* from the departure point for the current asteroid.

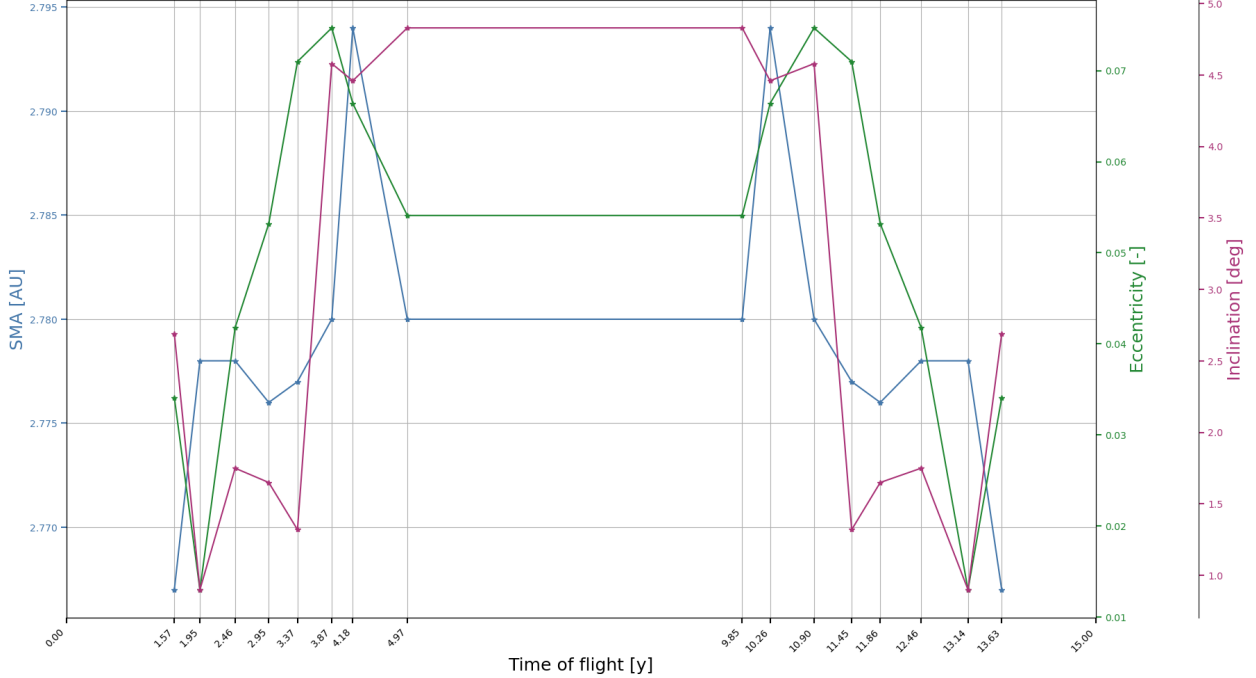


Figure 10: Orbital parameters (semi-major axis, eccentricity, and inclination) and for the orbits of the asteroids visited during the mission window for the chain at the bottom of Fig. 14. Note the symmetrical trajectory pattern that emerges naturally from the fact that during the collection phase (after coasting) the asteroids are visited in the opposite order to that of the miner deposition phase.

The resulting trajectory scaffolds are further optimised due to the cumulative estimation error for the backward mass. Despite this, scaffolds produced diverse trajectories that proved useful when constructing larger solutions. An example of one such scaffold is illustrated in Fig. 10.

5.2 A Beam Search that Looks Ahead in Time

An alternative approach, distinct from the one discussed earlier, relies on a modification to the standard Beam Search approach as outlined in [13]. In the following, we formally define the problem within the context of graph theory. Subsequently, we will delve into the algorithmic details of our heuristic solution.

A *configuration* of a spacecraft is an element of $\mathcal{A} \times \mathbb{R} \times \mathbb{R}$, that is, an asteroid at a given time with a given amount of (remaining) mass. Define the *configuration graph* of the mission as the directed graph D with vertex set $V(D) = (\mathcal{A} \times \mathbb{R} \times \mathbb{R}) \dot{\cup} \{E_s, E_t\}$ with E_s and E_t being two distinct vertices that represent the start and end at Earth. The (directed) edge set of D is defined as:

$$E(D) = \{ (x, y) \mid x, y \in \mathcal{A} \times \mathbb{R} \times \mathbb{R} \text{ and there is a hop from } x \text{ to } y \} \\ \cup \{ (E_s, x) \mid x \in \mathcal{D}_{\text{dep}} \} \cup \{ (x, E_t) \mid x \in \mathcal{D}_{\text{ret}} \}.$$

Here, a *hop* from (α, t, m) to (α', t', m') is a trajectory that brings a spacecraft that is rendezvoused with α at time t with a mass m to rendezvous with α' at time t' with a remaining mass of m' . Note that the graph D is infinite. However we may assume that D is given via an *oracle* that tells us whether a given hop is possible, which formally is a function:

$$\text{hop}: \mathcal{A} \times \mathbb{R} \times \mathbb{R} \times \mathcal{A} \times \mathbb{R} \times \mathbb{R} \rightarrow \{0, 1\}.$$

The concept of a “magic” oracle is well known and used in graph theory to formalize the mathematical structure of graph problems without focusing much on the specific problem domain. In our case the oracle encapsulate all space-flight mechanics knowledge that must be used in order to conclude whether a certain rendezvous (hop) is actually feasible and can be performed (in which case the edge exists) or not (in which case the edge is not there). The results from Section 4, as well as some book-keeping of the various masses collected, allow to code efficiently such an oracle in practice, without solving any optimal control problem. Observe that D is acyclic, as all edges go “along with time.” A path from E_s to E_t in D corresponds to a *multi-rendezvous* trajectory of a spacecraft that launches from Earth and returns to Earth at the end of the mission.

Of course, not all E_s - E_t -paths are equally contributing towards the mission’s objective. A common desire in multi-rendezvous missions is to rendezvous with as many asteroids as possible, which means that we need to find an E_s - E_t -path of maximum length such that no two vertices share the same \mathcal{A} -coordinate. This is a well-known NP-complete problem, even if D is finite and entirely given in the input.² The now *de facto* standard approach for solving multi-rendezvous problems is, thus, a heuristic version of a best-first search, called *beam search* [14]. The beam search explores D starting from E_s in the following sense: it maintains a list of active vertices (called the *beam*), which initially contains E_s . Then, the search is performed in phases, whereby every phase consists of two steps that explore D layer-by-layer:

Expansion first, every element in the beam is replaced by its neighborhood in $\mathcal{A} \times \mathbb{R} \times \mathbb{R}$;

Reduction then, a *score* is computed for every element in the beam and only the top β -elements are kept in the beam (hence, the beam has size at most β at the end of every phase).

This process is repeated until no element in the beam has any neighbor (because the configurations ran out of time or propellant). During the search, we keep track of configurations from which there is an edge to E_t so that, at the end, we can output the best one found. The parameter $\beta \in \mathbb{N}$ is called the *beamwidth* and (roughly) describes the quality of the search. If we set $\beta = 1$, the algorithm becomes a simple greedy search, and with increasing β , it converges towards an exact brute-force algorithm. Two technical details omitted in the above description are that, first, two configurations could lead to the same successor configuration and, thus, that we may explore the same part of D multiple times. This can be avoided by caching already explored configurations. Second, a vertex in D has an exceedingly large number of neighbors, which we can only partially explore. Hence, some heuristics must be used to reduce the neighborhood during the expansion step.

The parameter β (maximum beam size) can usually be determined relatively easily through experiments, while the heuristic to select neighbors falls into the domain of mission analysis and is heavily problem-dependent. In our experiments, for each element in the beam 1,000 target asteroids are selected using the orbital phasing indicator described in [14]. From these, a set of potential neighbours (low-thrust hops) is generated by gridding time from the minimum transfer time MINT (as computed by the MINTA2 approximation) for the following year in months increments.³

From an algorithm design perspective, a most interesting parameter of the algorithm is the *score* function used in the reduction step. If the goal is to “just” find a path that is as long as possible, reasonable scores are the amount of remaining time or mass, or a weighted combination of the two (see [13] for an extended discussion on multi-objective beam search in the context of mission analysis). However, this reasoning fails for the mission objective of GTOC12: Since a miner needs to be deployed *and* collected, the ships need to visit the same asteroid *twice*, at different epochs. This is precisely a property for which the beam search does *not* work well – the heuristic is supposed to make a locally good decision after all. We circumnavigated this issue by introducing the score shown in Listing 2, which tries to capture how easily the spacecraft can return, at some point in the future, to the same asteroid.

Formally, let f be a function that rates the quality of a hop – for instance, $f(h)$ could be the Δv required by the optimal low-thrust transfer for hop h or an approximation (the Lambert or the machine learned one); or it could be a phasing indicator [13, 5] i.e., not accounting for t' at all. Let us denote for a hop h the *reverse hop* with $\text{rev}(h)$, i.e., if h is a hop from α at time t to α' at time t' , then $\text{rev}(h)$ is the hop from α' at time t to α at time t' (masses are also swapped but are not relevant in what follows). Finally let $h \oplus T$ denote, for a hop h and a time duration T , the same hop in the future (e.g., $h \oplus 365.25$ would be the same hop in one year).

Figure 11 shows, as an example, the distribution of collected masses of ships found using the beam search with the score described in Listing 2 for the case that $f(h)$ is computed as an impulsive Lambert transfer (left) and using the orbital indicator [13, 5] (right). Overall, to create a large pool of promising self-sufficient ships, we performed multiple runs of the beam search: the histograms reported in Figure 11 are only an example of two runs that were performed at some point during the competition. Our experiments indicated that the scoring function f based on the orbital indicators performed the best on average. This was interpreted as an indication that the reverse hop score benefits from not depending explicitly on t' .

²The attentive reader may notice that D is acyclic and that, in acyclic graphs, the longest path problem can actually be solved in polynomial time. This is in general true, however, the additional constraint that we are not allowed to visit two vertices with the same \mathcal{A} -coordinate renders the problem NP-hard again.

³The grid [50, 100, 150, 200, 69π , 250] days was used in the last version of our experiments for reasons that are no longer obvious.

Listing 2: A scoring algorithm for a configuration (α_i, t_i, m_i) based on a function f that measures the quality of a hop (for instance, the Δv of an impulsive Lambert transfer). The value q_1 is the quality of the hop used to get to the configuration, and q_2 is the best quality a reverse hop has in the feature (at some fixed sampled dates).

```

1 algorithm future-score( $\alpha_i, t_i, m_i$ )
2    $h \leftarrow$  the hop that lead the beam search to  $(\alpha_i, t_i, m_i)$ 
3    $q_1 \leftarrow f(h)$ 
4    $q_2 \leftarrow \min\{f(\text{rev}(h) \oplus T \cdot 365.25) \mid T \in \{3, \dots, 9\}\}$ 
5   return  $q_1 + q_2$ 

```

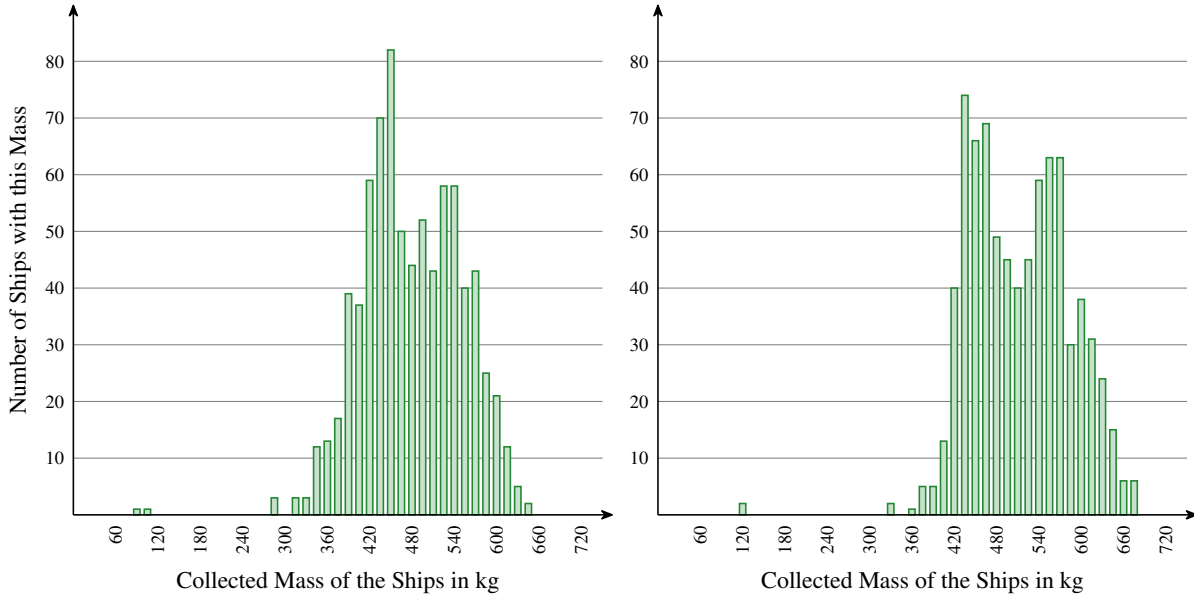


Figure 11: Distribution of the masses collected by ships found via one run of the beam search with the future-score. In the left plot, we show the distribution for the case that f simply computed the required Δv of the hop as impulsive Lambert transfer; in the right plot, f measures the quality of a hop using the orbital indicator [13, 5].

6 Selecting the Best Miners Subset

Since the algorithm developed in Section 5.2 is a heuristic, we can generate a diverse pool of single ships by varying the initial conditions. All in all, we found 371 *promising* ships, i. e., ships that collected a mass of at least 580kg and as high as 704kg. However, not all of these ships were independent, meaning that nothing prevented them from mining the same asteroid. Furthermore, asteroids that were already mined by previously submitted solutions suffered a penalty on their score according to the bonus function (see [2]). Towards the final days of the competition, both the above factors increasingly countered our efforts to improve the score of our solution. We thus experimented with methods to have our search algorithms (beam search and scaffolding search) produce ships that were guaranteed to avoid these issues. These included the black-listing of single asteroids from the searched data set, but also the forced exploration of different regions of the search space than those to which our algorithms were by design attracted to, via targeted searches on small subsets of \mathcal{A} containing around 200 asteroids. For instance, we observed a tendency towards approximately circular low-inclination trajectories for our best mass returning ships and hence searched subsets of \mathcal{A} formed by asteroids with orbits in thin elliptical or inclined tori. As the end of the competition was approaching fast, these methods were ad-hoc and delivered mixed results, but ultimately contributed a few ships to our final solution.

6.1 Combining Ships to a Full Solution of Maximized Score

As explained, the pool of *promising* ships, which exhibited dynamic growth and changes particularly in the concluding days of the competition, encompassed vessels with inherent incompatibilities and significant overlaps with selections made by other teams. This complexity rendered the straightforward selection of ships based on a naive collected mass ranking infeasible. To address this, we devised a method for identifying the optimal subset of ships from this pool.

The objective was to maximize the cumulative collected mass, accounting for penalties, while adhering to the crucial non-overlap condition. This intricate optimization problem was effectively mapped to an Integer Linear Program (ILP) for systematic resolution.

Formally, we associate with a ship σ_i a tuple $(m_i, s_i, \mathcal{A}_i)$ with $m_i, s_i \in \mathbb{R}^+$ being the *collected mass* of the ship and the *received score* (i. e., the mass after applying the bonus function), respectively. Let further $\mathcal{A}_i \subseteq \mathbb{N}$ be the set of IDs of asteroids visited by the ship.

Given a set $\mathcal{S} = \{(m_1, s_1, \mathcal{A}_1), \dots, (m_n, s_n, \mathcal{A}_n)\}$ of ships, our task is to find a set $I \subseteq \{1, \dots, n\}$ such that:

1. $\sum_{i \in I} s_i$ is maximized;
2. $\mathcal{A}_i \cap \mathcal{A}_j = \emptyset$ for all $i, j \in I$ with $i \neq j$;
3. $\frac{1}{|I|} \sum_{i \in I} m_i \geq \frac{\log(|I|/2)}{0.004}$.

That is, I is a selection of ships (which we call an *ensemble*) that maximizes the obtained score, and that is compatible in the sense that no two ships share an asteroid. The third item is the *average constraint* imposed by the competition, i. e., to use a certain number of ships, the average collected mass needs a certain value. Note that we optimize the score while the average constraint concerns the actual mass. See the left column in Figure 12 for an example.

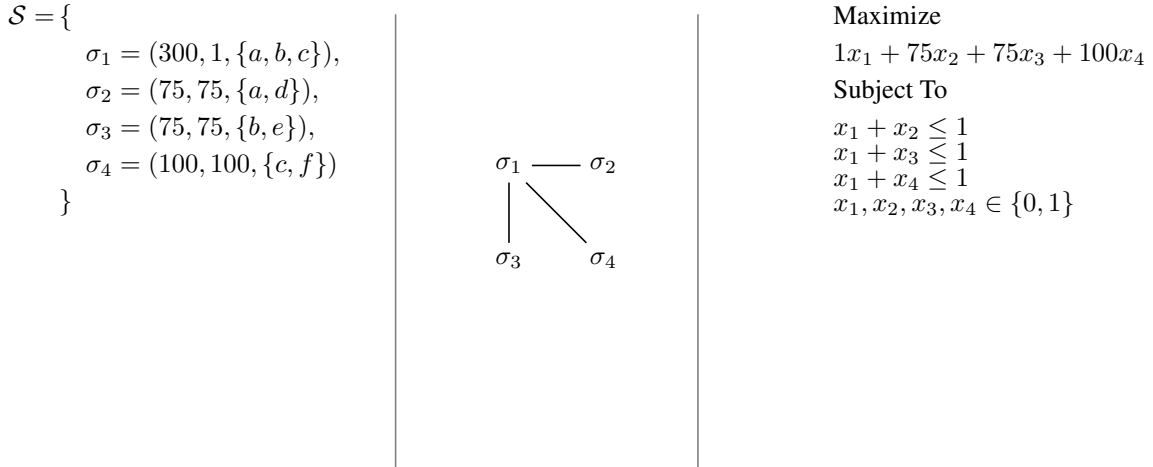


Figure 12: This figure illustrates an example instance of the problem of constructing an ensemble. The left column shows a set of four ships; the middle column shows the corresponding conflict graph (containing an edge between two ships if they use a common asteroid), and the right column shows our base encoding.

Our primary strategy to solve the problem is by encoding it as an *independent set* problem in the *conflict graph*. In detail, we construct a graph $G := G(\mathcal{S})$ with vertex set $V(G) = \mathcal{S}$ and edge set

$$E(G) = \{ \{(m, s, \mathcal{A}), (m', s', \mathcal{A}')\} \mid \mathcal{A} \cap \mathcal{A}' \neq \emptyset \}.$$

The center column of Figure 12 shows an incarnation of a conflict graph. Clearly, a score-optimal independent set (i. e., a set of pairwise non-adjacent vertices that maximizes the corresponding score) is exactly a solution to the first two items of the ensemble construction problem. In our running example, the score-optimal independent set is $\{\sigma_2, \sigma_3, \sigma_4\}$, achieving a score of 250. The example immediately illustrates the problem with this reasoning: While being score-optimal, the average mass of this solution is less than 84kg and, thus, violates the average constraint (the third item above). Alternatively, we may find it reasonable to compute a *mass-optimal* independent set, which, in Figure 12 is $\{\sigma_1\}$ with a glorious score of 1, which is not the best ensemble we can find.

We solved the problem using a two-pass algorithm utilizing 0-1-linear programming. In the first pass, we computed the maximum number of ships we could possibly add to the ensemble. To that end, we constructed the folklore LP for maximum-mass independent sets by introducing a *binary* variable x_i for every ship $\sigma_i \in \mathcal{S}$, maximizing $\sum_{i=1}^n x_i m_i$ under the constraints $x_i + x_j \leq 1$ for every two ships $\sigma_i, \sigma_j \in \mathcal{S}$ that share an asteroid. Let us denote this LP with Π . See the right column in Figure 12. To find the maximum number of simultaneously usable ships, we use the algorithm displayed in Listing 3.

Lemma 1. *If the algorithm from Listing 3 on input \mathcal{S} outputs a solution \mathbf{x} with $k := \sum_{i=1}^n x_i$, then it is possible to construct from \mathcal{S} an ensemble with k ships, but not with $k + 1$.*

Listing 3: An 0-1-LP-based algorithm to find the maximum number of ships in \mathcal{S} that can be added to an ensemble simultaneously. The algorithm is based on *row generation*, i. e., a sequence of similar LPs is generated by adding additional constraints (in Line 6) and incrementally solved (in Line 7).

```

1 algorithm maximum-number-of-ships( $\mathcal{S}$ )
2    $\Pi \leftarrow$  init LP from  $\mathcal{S}$ 
3    $\mathbf{x} \leftarrow$  optimal solution of  $\Pi$  // mass-optimal solution ...
4    $k \leftarrow \sum_{i=1}^n x_i$  // ... with  $k$  ships
5   while  $\frac{1}{k} \sum_{i=1}^n x_i m_i < \frac{k/2}{0.004}$  do // the solution violates the average-constraint
6      $\Pi \leftarrow \Pi \cup \sum_{i=1}^n x_i < k$  // search for a solution that uses less ships
7      $\mathbf{x} \leftarrow$  optimal solution of  $\Pi$ 
8      $k \leftarrow \sum_{i=1}^n x_i$ 
9   return  $\mathbf{x}$ 

```

Proof. The first direction is witnessed by \mathbf{x} and the fact that it passed the test in Line 5. For the second direction, consider the case that the algorithm has an intermediate solution \mathbf{x} of k ships that fails the test in Line 5. Then, any solution that satisfies the average constraint either collects more mass than $\sum_{i=1}^n x_i m_i$ or uses fewer ships. Since \mathbf{x} is mass-optimal by the definition of Π and the computed solutions in Line 3 or Line 7, there is no feasible solution in \mathcal{S} collecting more mass. Hence, the only way to fix the average mass is by using fewer ships, which is enforced in Line 6 by adding the cardinality constraint $\sum_{i=1}^n x_i < k$. \square

Once we know the maximum number k of ships, we compute a score-optimal independent set. Note that by Lemma 1 we do not need to consider ensembles with more than k ships. However, a score-optimal independent set may, of course, use fewer ships. The strategy is very similar: We construct an LP Π' that has the same variables and constraints as Π , and additionally has the cardinality constraint $\sum_{i=1}^n x_i \leq k$ (for the k we computed with Listing 3), and which has to maximize the objective function $\sum_{i=1}^n x_i s_i$ (note that we replaced “ m_i ” by “ s_i ”). We apply row generation again to find the global optimum; see Listing 4 for details. The algorithm differs from Listing 3 only in using the score-optimal LP, and by excluding only a single solution in lines 6 and 7 (instead of all solutions of size k).

Listing 4: An 0-1-LP-based algorithm that computes the score-optimal ensemble from a set \mathcal{S} of ships.

```

1 algorithm optimal-ensemble( $\mathcal{S}, k$ )
2    $\Pi' \leftarrow$  init LP from  $\mathcal{S}$  and  $k$ 
3    $\mathbf{x} \leftarrow$  optimal solution of  $\Pi'$  // score-optimal solution
4    $k \leftarrow \sum_{i=1}^n x_i$ 
5   while  $\frac{1}{k} \sum_{i=1}^n x_i m_i < \frac{k/2}{0.004}$  do // the solution violates the average-constraint
6      $I \leftarrow \{i \mid x_i = 1\}$  // index set of the solution
7      $\Pi' \leftarrow \Pi' \cup \sum_{i \in I} x_i < k$  // exclude the solution
8      $\mathbf{x} \leftarrow$  optimal solution of  $\Pi'$ 
9      $k \leftarrow \sum_{i=1}^n x_i$ 
10  return  $\mathbf{x}$ 

```

Theorem 2. *On input of \mathcal{S} and k , the algorithm from Listing 4 outputs the ensemble of the highest possible score encoded as binary vector \mathbf{x} .*

Proof. By Lemma 1, it is safe to work with Π' . Clearly, the output of the algorithm of Listing 4 is a solution since it is a solution of Π' and since it passes the average constraint in Line 5. To see that the solution is optimal, first observe that the initial \mathbf{x} computed in Line 3 is an upper bound on the solution since it is score-optimal. However, it may not be a feasible solution since it may violate the average constraint. Note that the best solution that satisfies the average constraint may use the same amount of ships as \mathbf{x} since Π' only optimizes for the score.

However, if \mathbf{x} fails the test in Line 5, we can conclude that no solution is a *superset* of (the set described by) \mathbf{x} . That is because every ship has a positive score and, hence, adding more ships would increase the score, contradicting the fact that \mathbf{x} was already score-optimal. Hence, by defining $k := \sum_{i=1}^n x_i$ and $I := \{i \mid x_i = 1\}$, and by adding the constraint $\sum_{i \in I} x_i < k$ to Π' , we exclude exactly one solution, namely \mathbf{x} . Repeatedly applying the argument to the solution computed in Line 8 establishes the claim of the theorem. \square

We remark that we could immediately compute an ensemble using the algorithm from Listing 4 (without using Listing 3), i. e., by setting $k = n$. However, there may be exponentially many solutions to Π' , while Listing 3 terminates after at most n rounds. In general, it is, thus, notably faster to run both algorithms in sequence, as described above. During the competition, we solved the integer linear programs in lines 3 and 7 in Listing 3, and in lines 3 and 8 in Listing 4 using the open-source solver SCIP [9].

6.2 Automatic Removal of Asteroids

Some of the ships (m, s, A) computed in Section 5.2 had the unfortunate property that they harvested just the bare minimum of mass from an asteroid $a \in A$ that was heavily penalized by the bonus function. This property is deplorable if (i) the ship is in general good (s and m are large), and (ii) there is another good ship (m', s', A') with $A \cap A' = \{a\}$. In this case, we would eventually like to add both ships to our final solution while removing a from one of the trajectories and gluing the, now broken, branches. Note that it is generally not easy to automatically change a ship’s trajectory to include other asteroids, but removing one from the trajectory is trivial. We can adapt Π' to find removable asteroids as follows: We keep the indicator variables x_i for every ship $\sigma_i \in \mathcal{S}$ and introduce additional binary variables x_i^a for every asteroid $a \in A_i$ (with the semantic “remove asteroid a from ship σ_i ”). For every pair of ships $\sigma_i, \sigma_j \in \mathcal{S}$ with $i \neq j$ and $A_i \cap A_j \neq \emptyset$ we replace the constraints $x_i + x_j \leq 1$ by the following constraints for every $a \in A_i \cap A_j$:

$$-x_i + -x_j + x_i^a + x_j^a \geq -1.$$

This constraint can be read as: “Either ship σ_i or ship σ_j is not in the ensemble, or asteroid a is removed from at least one of the ships”. Of course, if we remove an asteroid, the score obtained by a ship is reduced. Let r_i^a denote the score that ship σ_i obtains from harvesting asteroid a , then the new objective function is:

$$\text{maximize } \sum_{i=1}^n x_i s_i - \sum_{i=1}^n \sum_{a \in A_i} x_i^a r_i^a.$$

We can update Listing 4 by replacing Π' with the LP described above. The output will then be a score-optimal ensemble (described by the values of the x_i) together with the precise information on which asteroids need to be removed from which ships (encoded by the x_i^a).

7 The Final Assembled Solution

Figure 13, kindly provided by the competition organizers [2] gives an overview of our team’s final solution found applying the selection procedure described in Sect. 6 to the pool of 371 ships able to return more than 580kg from the various runs of the search algorithms outlined in Sect. 5 and a local refinement step applied to adjust the various epochs as to maximize the overall collected mass of each self-contained ship. The solution consists of 28 ships collectively mining 18 475 kg of material from 249 asteroids, resulting in a total score of 15 728 (including bonus coefficients). The ship selection algorithm, when ignoring the bonus coefficient, returns a different selection corresponding to a slightly better solution at 18 562 kg, signaling the robustness and diversity of our final ship pool to the solutions found by other teams during the competition.

As mentioned previously, a consequence of our search procedure (described in Sect. 5) is that all ships are self-contained, in that each of them collects material from the same asteroids on which they deployed miners. Each ship performs rendezvous with seven to ten asteroids twice during the mission. The bird’s-eye view of the trajectories in the xy plane in Fig. 13 showcases that most mining activity occurs in the high asteroid density region between 2.7 and 3 AU (see Fig. 1). Some of the outliers in this respect correspond to ships resulting from targeted searches on thin elliptical or inclined torus subsets of \mathcal{A} (Sect. 6). Of note is that none of the 28 selected ships made use of a Mars or Venus gravity assist.

Table 1 lists for each of the 28 ships constituting our solution their contribution to the final score, the collected mass, the set of visited asteroids, the search algorithm that produced them, and the associated figure. In total five of the ships selected were produced by the scaffolding algorithm (Sect. 5.1) and 23 by the beam search (Sect. 5.2). This discrepancy should however not be interpreted in terms of algorithm quality, since we also launched a disproportionately larger amount of searches with the beam search.

In the top panel of Fig. 14 we take a closer look at our ship with the highest score of 618 by means of an $r(t)$ plot. It is a product of a beam search on a thin elliptical torus subset of \mathcal{A} around the orbit of the initially rendezvoused asteroid. Due to this restricted search space, all rendezvoused asteroids are on orbits with similar characteristics, and the ship finds smooth transitions between them. As discussed at the beginning of Sect. 6, the search space restriction was an ad-hoc attempt to limit the impact of bonus coefficients by forcing the beam search to explore trajectories which it

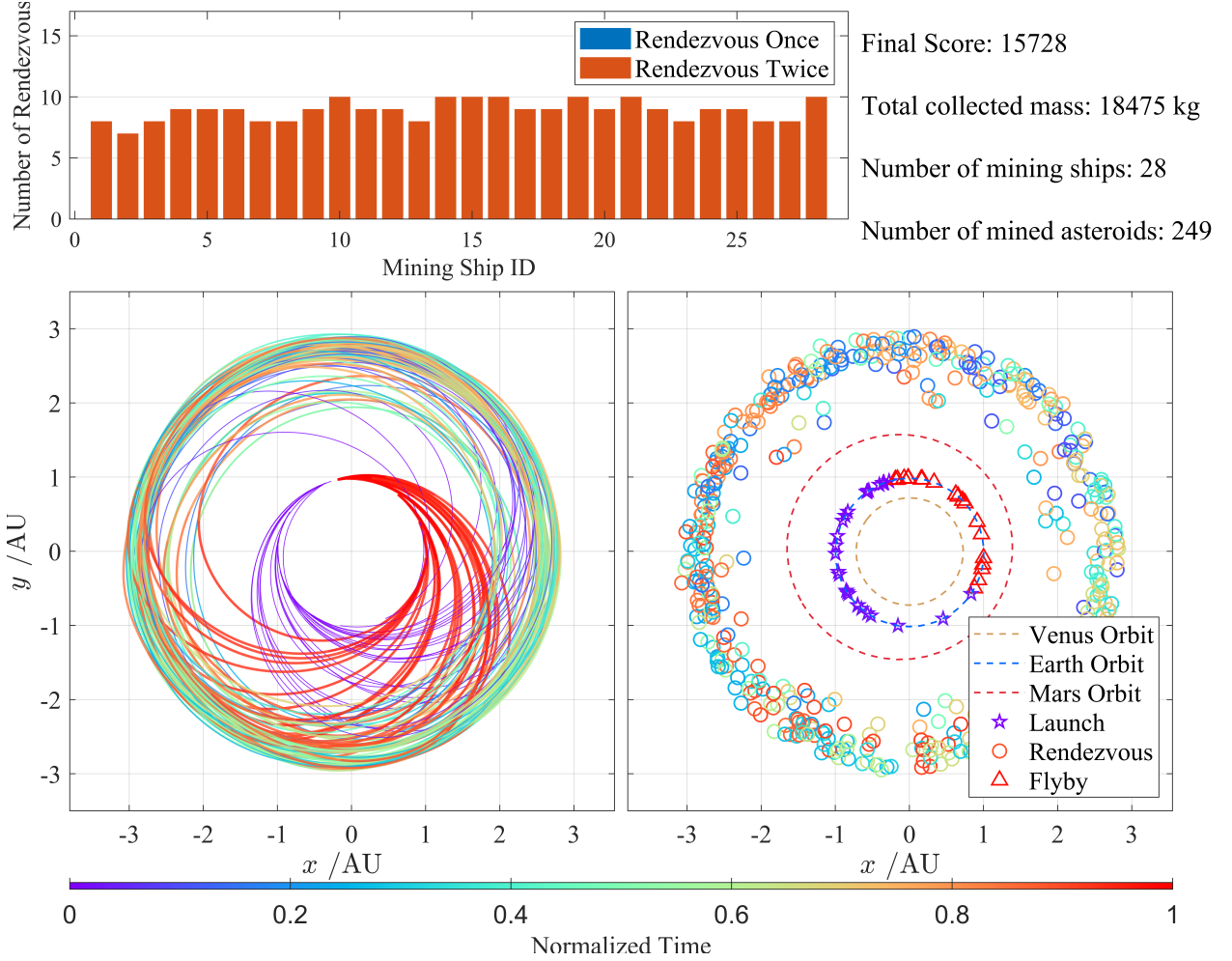


Figure 13: Top: Number of rendezvous with an asteroid per ship. Since our solution is comprised solely of self-contained ships, each asteroid is rendezvoused twice by the same ship. Bottom: Projection of the trajectories of our solution (left) and of events (right) into the ecliptic. The temporal dimension is colour coded. Source: <https://github.com/GTOC12-official/>.

would otherwise rate unfavourably (in this case elliptical ones) and indeed the collected mass for this ship translates unaffected into score. It is important to stress however, that such ships could not have made up the bulk of our solution, since their collected mass is low. Higher mass collecting ships were required to allow for a 28 ship solution and avoid bottlenecks.

The middle panel of Fig. 14 shows the $r(t)$ plot of the ship of our solution with the highest mass return of 699 kg, which is a product of the beam search. Here the unconstrained search space allowed the algorithm to find and efficiently mine the high density region just below 3 AU (Fig. 1). Apart from outliers, the rendezvous cluster in the beginning (deployment) and end phases (collection) of the mission are interpreted as consequences of the look-ahead heuristics of the beam search.

Finally, the bottom panel of Fig. 14 shows the $r(t)$ plot of the highest mass returning ship produced by the scaffolding algorithm. Also, this ship was attracted to efficiently mine in the high density region. By construction, the asteroids are rendezvoused approximately symmetrically around a central period in which the ship is coasting on an asteroid. The algorithm seeks to maximise this coasting period, and to achieve this, the ship invests in relatively expensive thrusts.

What all the above examples have in common is a low fluctuation in semi-major axis, and hence in period, of the rendezvoused asteroids. This is in part a consequence of the energy-efficient transfers found by the algorithms as well as of the fact that similar periods ease the opportunities for revisits, in particular for near-circular trajectories.

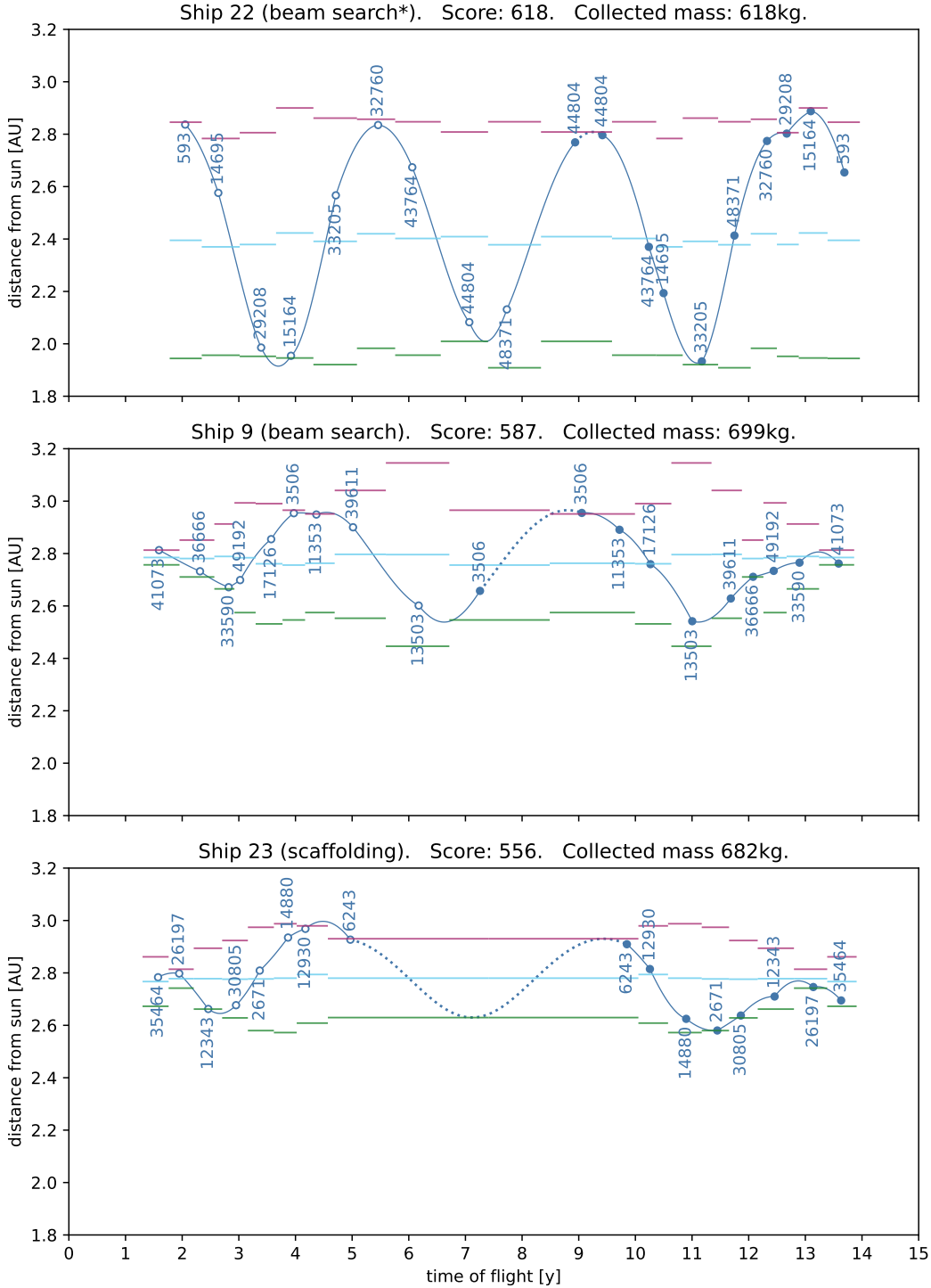


Figure 14: Plots of $r(t)$ of the highest scoring ship (top) and of the highest mass returning ships produced by the beam search (middle) and scaffolding algorithm (bottom). Full/empty circles indicate deployment/pickup rendezvous with the labeled asteroids. Transfers are plotted solid, coastings on an asteroid dotted. The semi-major axis, the pericentre distance, and the apocentre distance of the rendezvoused asteroids are indicated by the blue, green, and red bars respectively. The chosen range on the distance axis is common to all three plots to ease a direct comparison of the geometries of the trajectories.

Table 1: Properties of the 28 ships of our solution: the score, the collected mass, the number of visited asteroids, and the source algorithm that produced them. ‘Scaffolding’ and ‘beam search’ refer to the algorithms of Sects. 5.1 and 5.2, respectively. An asterisk marks targeted searches on small subsets of \mathcal{A} , as discussed in Sect. 6.

<i>Ship</i>	<i>Score</i>	<i>Mass</i>	<i>Asteroids</i>	<i>Algorithm</i>	<i>Figures</i>
1	542	649 kg	8	scaffolding	
2	549	613 kg	7	scaffolding	
3	565	659 kg	8	beam search	
4	554	687 kg	9	beam search	
5	586	586 kg	9	beam search*	
6	573	698 kg	9	beam search	
7	543	653 kg	8	scaffolding	
8	595	610 kg	8	beam search*	
9	587	699 kg	9	beam search	Figure 14 middle
10	537	659 kg	10	beam search	
11	541	645 kg	9	beam search	
12	562	695 kg	9	beam search	
13	538	653 kg	8	beam search	
14	565	670 kg	10	beam search	
15	560	686 kg	10	beam search	
16	564	643 kg	10	beam search	
17	567	661 kg	9	beam search	
18	567	661 kg	9	beam search	
19	547	655 kg	10	beam search	
20	568	683 kg	9	beam search	
21	570	697 kg	10	beam search	
22	618	618 kg	9	beam search*	Figure 14 top
23	556	682 kg	8	scaffolding	Figures 10 and 14 bottom
24	565	660 kg	9	beam search	
25	559	666 kg	9	beam search	
26	555	641 kg	8	scaffolding	
27	545	653 kg	8	beam search	
28	555	693 kg	10	beam search	

The two highest mass returning ships that were found during the competition collected 704 kg of ore. These ships, however, were not selected for the submitted solution due to the presence of highly desirable and targeted asteroids in them, resulting in a harsh penalty induced by bonus coefficients.

8 Conclusions

The low-thrust multiple-rendezvous trajectories designed for the asteroid mining mission featured in the 12th edition of the Global Optimization Competitions can be well approximated by a first-order correction to their purely ballistic representation. This approximation offers significant efficiency advantages during the exploration of the vast combinatorial search space. It enables the avoidance of solving complex optimal control problems and instead facilitates the use of Lambert’s arc computations for the trajectory analysis. Furthermore, we found that ignoring the collaborative aspect of the mining mission and focusing on the design of self-sufficient ships, mining and collecting all resources, allows to find ships returning > 700 kg of mined resources, albeit not consistently.

9 Acknowledgment

The authors wish to extend our sincere gratitude to Carlo Cavazzoni, Alessandro Russo, Sciarappa Antonio, and Franco Ongaro for their assistance in facilitating access to the Leonardo computing infrastructure in the weeks leading up to the competition. Although it turned out to be unnecessary for the particular strategy we devised, we nevertheless appreciated the opportunity and support provided.

References

- [1] Dario Izzo. 1st ACT global trajectory optimisation competition: Problem description and summary of the results. *Acta Astronautica*, 61(9):731–734, 2007.
- [2] Z. Zhang, N. Zhang, X. Guo, D. Wu, X. Xie, J. Yang, F. Jiang, and H. Baoyin. Sustainable asteroid mining: on the design of the gtoc12 problem and summary of the results. *Astrodynamics, this issue*, 2024.
- [3] Jon Sims, Paul Finlayson, Edward Rinderle, Matthew Vavrina, and Theresa Kowalkowski. Implementation of a low-thrust trajectory optimization algorithm for preliminary design. In *AIAA/AAS Astrodynamics specialist conference and exhibit*, page 6746, 2006.
- [4] Philip E Gill, Walter Murray, and Michael A Saunders. SNOPT: An SQP algorithm for large-scale constrained optimization. *SIAM review*, 47(1):99–131, 2005.
- [5] Hennes, Daniel and Izzo, Dario and Landau, Damon. Fast approximators for optimal low-thrust hops between main belt asteroids. In *2016 IEEE Symposium Series on Computational Intelligence (SSCI)*, pages 1–7, 2016.
- [6] Zhong Zhang, Nan Zhang, Xiang Guo, Di Wu, Xuan Xie, Jinyuan Li, Jia Yang, Shiyu Chen, Fanghua Jiang, Hexi Baoyin, et al. Gtoc 11: Results from tsinghua university and shanghai institute of satellite engineering. *Acta Astronautica*, 202:819–828, 2023.
- [7] Adam Paszke, Sam Gross, Francisco Massa, Adam Lerer, James Bradbury, Gregory Chanan, Trevor Killeen, Zeming Lin, Natalia Gimelshein, Luca Antiga, et al. Pytorch: An imperative style, high-performance deep learning library. *Advances in neural information processing systems*, 32, 2019.
- [8] Dario Izzo. PyGMO and PyKEP: Open source tools for massively parallel optimization in astrodynamics (the case of interplanetary trajectory optimization). In *Proceedings of the Fifth International Conference on Astrodynamics Tools and Techniques, ICATT*. sn, 2012.
- [9] Ksenia Bestuzheva, Mathieu Besançon, Wei-Kun Chen, Antonia Chmiela, Tim Donkiewicz, Jasper van Doornmalen, Leon Eifler, Oliver Gaul, Gerald Gamrath, Ambros Gleixner, Leona Gottwald, Christoph Graczyk, Katrin Halbig, Alexander Hoen, Christopher Hojny, Rolf van der Hulst, Thorsten Koch, Marco Lübbecke, Stephen J. Maher, Frederic Matter, Erik Mühmer, Benjamin Müller, Marc E. Pfetsch, Daniel Rehfeldt, Steffan Schlein, Franziska Schlösser, Felipe Serrano, Yuji Shinano, Boro Sofranac, Mark Turner, Stefan Vigerske, Fabian Wegscheider, Philipp Wellner, Dieter Weninger, and Jakob Witzig. Enabling research through the scip optimization suite 8.0. *ACM Trans. Math. Softw.*, 49(2), 2023.
- [10] Massimiliano Vasile and Paolo De Pascale. Preliminary design of multiple gravity-assist trajectories. *Journal of Spacecraft and Rockets*, 43(4):794–805, 2006.
- [11] Dario Izzo. Revisiting lambert's problem. *Celestial Mechanics and Dynamical Astronomy*, 121:1–15, 2015.
- [12] Richard H Battin. *An introduction to the mathematics and methods of astrodynamics*. AIAA, 1999.
- [13] D. Izzo, D. Hennes, L.F. Simoes, and M. Märten. *Designing complex interplanetary trajectories for the global trajectory optimization competitions*, chapter 8, pages 151–176. Wiley, New York, 2016.
- [14] Luís F Simões, Dario Izzo, Evert Haasdijk, and AE Eiben. Multi-rendezvous spacecraft trajectory optimization with beam P-ACO. In *Evolutionary Computation in Combinatorial Optimization: 17th European Conference, EvoCOP 2017*, pages 141–156, 2017.